NASA-CR-193815

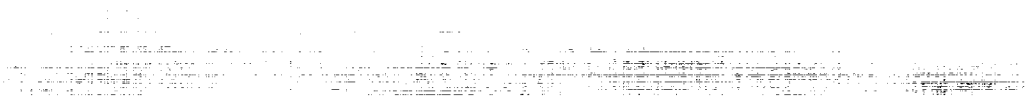

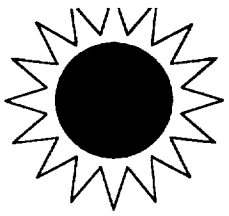

HIGH ALTITUDE OBSERVATORY **53 Years • 1940-1993**

NATIONAL CENTER FOR ATMOSPHERIC RESEARCH
PO Box 3000; Boulder, Colorado 80307-3000
Telephone: (303) 497-1574; *Telefax*: (303) 497-1589; *Telex*: 989764
Internet: woods@virgo.hao.ucar.edu; *DECnet/SPAN*: VIRGO::WOODS

April 26, 1994

NASA Scientific and Technical Information Facility
Accessioning Dept.
800 Elkridge Landing Rd
Linthicum Heights, MD 21090

SUBJECT: Final Report for NASA Grant NASA-S97242-E (previously NAG5-1505)

Dear Sir:

The analysis of the solar spectral irradiance from the Airglow-Solar Spectrometer Instrument (ASSI) on the San Marco 5 satellite is the focus for this research grant. After many iterations with the several co-investigators, our paper describing the calibrations of and results from the San Marco ASSI is now ready for submission. A pre-print copy of this paper is enclosed. The calibration of the ASSI included (1) transfer of photometric calibration from a rocket experiment and the Solar Mesosphere Explorer (SME), (2) use of the on-board radioactive calibration sources, (3) validation of the ASSI sensitivity over its field of view, and (4) determining the degradation of the spectrometers. The results concerning the solar irradiance variability are somewhat limited by the quality and quantity of the ASSI solar data. The typical solar measurements from ASSI has a precision of about 10%, and the amount of solar variability for most solar emissions expected during the San Marco mission is only 10%. In addition, only 16 full-spectrum measurements of the Sun were made during the San Marco mission instead of the more desirable frequency of daily measurements. Nonetheless, we have determined that (1) the absolute values for the solar irradiance needs adjustment in the current proxy models of the solar UV irradiance and (2) the amount of solar variability from the proxy models are in reasonable agreement with the ASSI measurements.

This research grant also has supported the development a new solar EUV irradiance proxy model. We expect that the magnetic flux is responsible for most of the heating, via Alfén waves, in the chromosphere, transition region, and corona, so we first set out to establish that the photospheric magnetic fluxes can be a good index for the chromospheric and coronal emissions. A comparison between photospheric magnetograms [Kitt Peak, J. Harvey] and images of chromospheric emissions [i.e., Ca K, H α, He 10830 Å from Kitt Peak, J. Harvey] lead to the parameterization that the chromospheric emissions from the active regions vary as the magnetic field to the 1/2 power. The comparison of the photospheric magnetograms to images of the coronal emissions suggests that the coronal emissions vary as the magnetic flux (to the 1.0 power); however, we have more work in these coronal comparisons because the magnetic field arising from the photosphere does change its structure more by the time is reaches the corona than it does in the chromosphere. Because we expect that the strongest magnetic fields to quickly penetrate the chromosphere and thus have a proportionally less effect on the chromosphere, we then studied the differences in radiation levels for different magnetic field levels. From examining time series of solar irradiance data and magnetic fields at different levels, we did indeed find that the chromospheric emissions correlate best with the moderate magnetic field levels and that the coronal emissions correlate best with the large magnetic field levels.

We are currently working on how to best parameterize these results for the new proxy model. We are trying to optimize both accuracy of the model and simplicity in using the model. One approach that employs a five parameter proxy model seems to be optimal at this time. Two parameters are derived from the magnetic flux images, and three parameters are wavelength dependent and are empirically derived using solar irradiance measurements. The spectral coverage for this model is 0.5 to 200 nm and is the spectral region most important to upper atmospheric studies above 50 km. The time step for this proxy model is one day and is satisfactory for most solar-terrestrial studies. Because the existing solar EUV irradiance data sets (mainly AE-E and San Marco) lack the accuracy and spectral and temporal coverage needed for precisely deriving the three wavelength dependent parameters, other, more accurate data sets, such as from the UARS SOLSTICE, have been used to verify the proxy model at the longer wavelengths above 120 nm. The current proxy model is able to reproduce the UARS SOLSTICE measurements with an accuracy of about 3% (1 σ) as shown in Figure 1 for the Lyman α irradiance. A challenging part left of this proxy model development is to derive the remaining parameters at the shorter wavelengths. We realize that these shorter wavelength parameters will not be as accurate as we desire, but they will have to suffice for now until more precise solar EUV irradiance time series are available. From initial examination of this proxy model at shorter wavelengths, we expect an accuracy for the proxy model near 10%. Because existing proxy models have an accuracy of about 30%, we feel that this new proxy model is an improvement and should be significantly better once more precise solar EUV irradiance data are available.

This grant has largely supported John Worden, a University of Colorado graduate student, in analyzing the San Marco ASSI data and in developing a new proxy model of the solar UV irradiance. This grant has also supported our efforts in establishing reference solar spectra for the SOLERS 22, an international STEP program chaired by Dr. Richard Donnelly. The papers and presentations supported by this grant are listed on the following page.

We consider the ASSI solar data analysis complete and thus have meet our primary goal for this research grant. Our secondary goal to develop an improved proxy model of the solar UV irradiance is well underway and we expect the first version of the model to be released within a year. More precise measurements of solar UV irradiance, such as from the TIMED mission, are critically needed before we (or anybody else) can make significantly better proxy models; thus, our proxy model development will be an on-going process as better solar irradiance data are available. Our current suborbital program, started in April 1994, will provide solar irradiance measurements and additional support for proxy model development.

We thank NASA Headquarters and NASA GSFC for supporting this Guest Investigator research program.

Sincerely,

Thomas N. Woods

Thomas N. Woods,
Principal Investigator

LISTING 1. Papers, Presentations and Students Supported by NASA Grant NASA-S97242-E (previously NAG5-1505).

Papers

Worden, J., T. Woods, G. Rottman, G. Schmidtke, H. Tai, H. Doll, and S. C. Solomon, Calibration of and results from the Airglow Solar Spectrometer Instrument aboard the San Marco 5 satellite, *J. Geophys. Res.*, to be submitted, 1994.

Tobiska, W. K., G. Schmidtke, H. Doll, T. N. Woods, J. Worden, and S. Chakrabarti, "Comparisons of San Marco ASSI solar EUV and EUV91 model", *Adv. Space Res.*, in press, 1994.

Schmidtke, G., T. N. Woods, J. Worden, H. Doll, S. C. Solomon, and G. J. Rottman, "Solar EUV irradiance from the San Marco ASSI: a reference spectrum", *Geophys. Res. Letters*, **19**, 2175-2178, 1992.

Woods, T. , "Working group 4 and 5 report for 1991 SOLERS 22 workshop", Proc. of SOLERS 22 Workshop, D. Donnelly (editor), 460-467, 1992.

Presentations

Woods, T. N., S. Bailey, S. Solomon, G. Rottman, and J. Worden, Recent solar EUV irradiance measurements, *Front Range Am. Geophy. Union* , p. 16, Feb. 14-15, 1994.

Woods, T. N, J. Worden, G. J. Rottman, S. C. Solomon and G. Schmidtke, Observed variability of the solar EUV irradiance, *The Sun as a Variable Star,* IAU #143, Boulder, 198, 1993.

Worden, J. and T. Woods, Calibration of the San Marco ASSI EUV and UV spectrometers, Ninth Workshop on the Vacuum Ultraviolet Calibration of Space Experiments, Boulder, CO, March 10-11, 1993.

Worden, J, T. N. Woods, G. J. Rottman, S. C. Solomon, G. Schmidtke, Observed solar cycle variability of the solar EUV irradiance, *Am. Geophy. Union* , **73 (43)**, 436, 1992.

Worden, J., T. Woods, G. Schmidtke, and G. Rottman, Solar Variability during the San Marco mission, San Marco Science Team Meeting, Rome, Italy, 1992.

Woods, T. N., G. Schmidtke, J. Worden, H. Doll, S. C. Solomon, K. Tobiska, and G. J. Rottman, Recent results of solar EUV irradiance research, STEP Symposium / COSPAR Colloquium, p. 35, Aug 1992.

Schmidtke, H. Doll, C. Wita, T. Woods, J. Worden, S. C. Solomon, and G. J. Rottman, Solar EUV irradiance variability measured by the San Marco ASSI, *Annales Geophysicae*, **10 (III)**, C-369, 1992.

Woods, T. and G. Rottman, Solar UV variability, San Marco Science Team Meeting, Dallas, Texas, 1991.

Schmidtke, G., T. Woods, H. Doll, S. C. Solomon, J. Worden, C. Wita, and G. Rottman, Solar EUV irradiance variability measured by the San Marco ASSI: calibrations and results, IAGA, 1991.

Students

John Worden, a graduate student at the University of Colorado, has worked on this research program from June 1991 to the present. John has analyzed the San Marco ASSI solar data and is developing an improved proxy model of the solar UV irradiance. These two topics are the main emphasis for his PhD dissertation, which is expected to be completed in about one year.

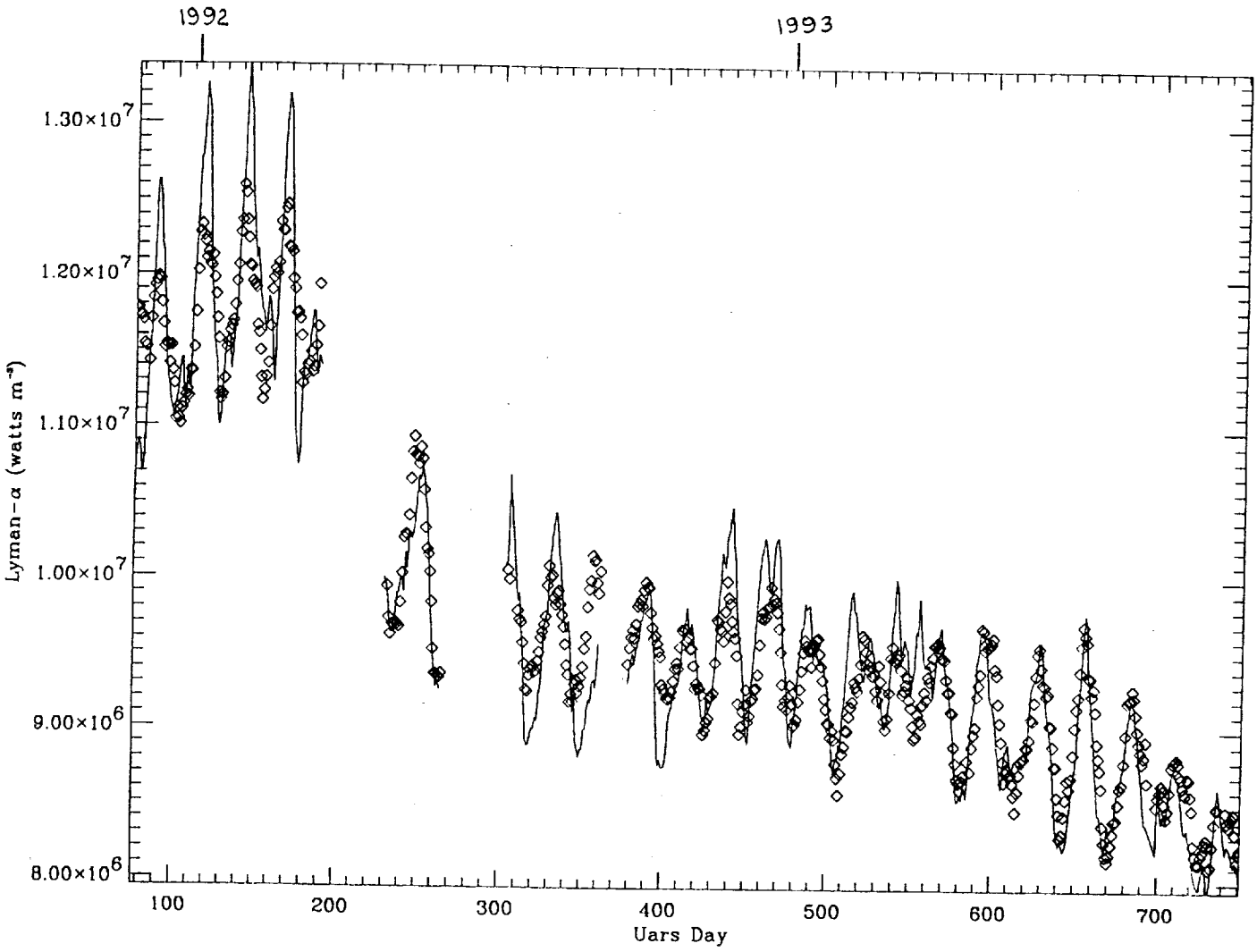

Figure 1. Measurements and Model Predictions for Solar Lyman α Irradiance. The measurements, shown as the solid line, is from the Upper Atmosphere Research Satellite Solar Stellar Irradiance Comparison Experiment (UARS SOLSTICE; PI: Gary Rottman). The proxy model predictions for the Lyman α irradiance, shown as the diamond symbols, use the Kitt Peak NSO photospheric magnetograms (PI: Jack Harvey) to calculate the daily chromospheric indices. The RMS difference between the measurements and the model predictions is 2.7%. The gaps in the time series are at the times when either SOLSTICE Lyman α measurements or the NSO magnetogram measurements were not made.

Calibration of and Solar Results from the San Marco Airglow - Solar Spectrometer Instrument in the Extreme Ultraviolet

John Worden, Tom Woods, Gary Rottman
High Altitude Observatory, National Center for Atmospheric Research

Gerhard Schmidtke, Hongsheng Tai
Fraunhofer-Institut fur Physikalische Meβtechnik

Harry Doll
Physikalisch-Technische Studien G.M.B.H.

Stanley C. Solomon
Laboratory for Atmospheric and Space Physics, University of Colorado

Abstract. The San Marco 5 satellite, launched in early 1988 and lasting for about nine months, carried the Airglow-Solar Spectrometer Instrument (ASSI). This eighteen channel spectrometer measured the solar and terrestrial radiations in the wavelength region between 20 and 700 nm. An absolute photometric calibration for the ultraviolet channels is determined primarily using the solar irradiance from a rocket experiment and the Solar Mesosphere Explorer (SME). On-board radioactive sources that monitored the sensitivity degradation of the extreme ultraviolet (EUV) channels and comparisons of solar irradiance from overlapping channels completed the calibration. Exponential curves adequately describe the sensitivity changes of the optics and detectors and are fitted to several solar emission time series to establish the temporal calibration for the ASSI EUV channels. Several emission features are extracted from the ASSI data set, and their irradiance as a function of time are compared to current solar EUV proxy models. It is found that systematic differences exist between the absolute value of the EUV irradiance measured by the ASSI and the corresponding irradiance predictions from the proxy models.

1. Introduction

Since 1980 there has been very little solar radiometry in the extreme ultraviolet (EUV). The Atmosphere Explorer-E (AE-E) spacecraft measured the solar EUV irradiance from 1976 to 1980 during the ascending phase of solar cycle 21. This data set provided an almost complete description of solar cycle 21 and also allowed the creation of proxy models to predict solar EUV emissions [i.e. *Hinteregger et al.*, 1981]. Such proxy models are of importance for topics in the physics of the Earth's upper atmosphere at times when no measurements exist of the solar EUV irradiance. The accuracy of the current proxy models is limited partly by the lack of in-flight calibration of the AE-E solar instrument and the choices for the proxies. The estimated one sigma uncertainty for the *Hinteregger et al.*, [1981] and *Tobiska* [1991] models is about 30%. The Airglow Solar Spectrometer Instrument (ASSI) was the only satellite instrument to measure the Earth airglow and solar spectral irradiance during solar cycle 22. These data check the consistency of current proxy models during a different solar cycle and add to our understanding of solar EUV variability.

This paper presents a brief description of the ASSI experiment, results of the temporal calibration for the ASSI EUV channels and an analysis of the solar EUV variability including comparisons to predicted values from Hinteregger's solar proxy model predictions [*Hinteregger et al.*, 1981] and from Tobiska's EUV91 model [*Tobiska et al.*, 1991]. *Schmidtke et al.*, [1985] provides a detailed instrument description of the ASSI and *Schmidtke et al.*, [1992] presents an solar EUV irradiance reference spectrum for November 10, 1988.

2. Instrumentation

The ASSI is composed of four Rowland circle grating spectrometers each having four or five detectors. The spectral coverage of the ASSI is from 20 to 700 nm with spectral resolution ranging from 1 to 3 nm. The four spectrometers are grouped into two components, ASSI A and B, composed of nine channels each. The calibration of and solar results from the ASSI channels 12, 16 and 18 are presented in this paper. The spectral resolution and effective wavelength range of each of these EUV channels are listed in Table 1. The photometric calibration for the other ASSI channels are still being characterized.

3. Instrument Calibrations

3.1 Photometic Calibration

As described by *Schmidtke et al.*, [1992], the primary photometric calibration for the ASSI EUV channels is defined on November 10, 1988 using a solar reference spectrum from a sounding rocket experiment [*Woods and Rottman*, 1990], which measured the solar EUV irradiance from 30 nm to 110 nm, and from the SME solar measurements above 115 nm. The first step in determining the November 10 ASSI calbration parameters is to calculate the solar flux for November 10 using the ASSI pre-flight calibration. This flux is corrected for atmospheric absorption using the optical depth calculated with atmospheric densities from the MSIS-86 model [*Hedin* , 1987], and cross sections for N_2, O_2 and O from *Fennelly and Torr* [1991] and *Conway* [1986]. If the uncertainty in the atmospheric correction is greater than 20%, the measurement is not used, and whenever possible, redundant measurements are averaged. To obtain the calibration parameters, the stronger emission features are compared to the reference spectrum. This calibration at a few wavelengths per channel is extended to all wavelengths using interpolations and/or polynomial fits. These refined calibration parameters are verified by comparing irradiances from overlapping channels. Figure 1 presents the sensitivity on November 10 1988 as a function of wavelength for each of the EUV channels; these sensitivities are all similar as the gratings and detectors are similar. The revised sensitivities also show similar wavelength dependence as the pre-flight calibrations.

The on-board beta particle sources also provide information for the photometric calibration by tracking the EUV detector sensitivities. Because of changes in the grating efficiencies since the pre-flight calibration, this tracking method does not give complete knowledge of the sensitivity changes for the ASSI EUV detectors and optics. There is however a good correlation between the change in the detector sensitivity at EUV wavelengths and the detector sensitivity at wavelengths near 55 nm [*Schmidtke et al.*, 1992]. The change in the detector sensitivity for each of the EUV channels as seen by the radioactive sources are shown in Figure 2.

3.2 ASSI Lyman-α Calibration

A special photometric issue for the ASSI is the calibration at Lyman-α (121.6 nm). Use of the SME Lyman-α measurements to calculate the channel 18 calibration parameters produces a "bump" on the channel 18 calibration curve that is inconsistent with the shape of

the pre-flight calibration curve. The bump can be removed by fitting a sixth order polynomial to the revised channel 18 calibration curve and attributing a weight of zero in the fitting routine to the bump section. In this manner, the channel 18 calibration parameters for Lyman-α are normalized to the rocket spectra. The Lyman-α solar irradiance measured by the ASSI using these updated calibration parameters is found to be 5.8×10^{11} photons cm^{-2} s^{-1}. The three different channel 18 sensitivities are presented in Figure 3.

The recent solar UV measurements from the Upper Atmosphere Research Satellite (UARS) provides additional information about the Lyman-α irradiance. The solar UV instruments aboard the UARS are the Solar Stellar Irradiance Comparison Experiment (SOLSTICE) and the Solar Ultraviolet Spectral Irradiance Monitor (SUSIM). Modeling of the UARS SOLSTICE Lyman-α measurements with various solar indices such as the Kitt Peak He I 10830 equivalent widths, NOAA Mg II core to wing ratios, Ottawa F10.7 solar radio flux, and Kitt Peak magnetic field measurements suggest that the Lyman-α solar irradiance on November 10, 1988 should also be about 5.8×10^{11} photons cm^{-2} s^{-1} instead of 3.35×10^{11} photons cm^{-2} s^{-1} as derived from the SME. Validation of the UARS SOLSTICE measurements with the UARS SUSIM measurements, as well as earlier AE-E measurements also support these higher Lyman-α values. Simultaneous measurements with the SME and UARS solar instruments do however suggest that some of the differences is solar variability and not all related to calibration differences. Both the Pioneer Venus Langmuir Probe measurements [*Hoegy et al.*, 1993] and rocket NO ionization cell measurements [*Woods and Rottman*, 1990] each agree with the SME and UARS measurements to within their calibration uncertainty of 30%. At this time, we believe there may be a 20% anomalous solar variability effect and a 50% instrument calibration difference. Continued validation of these Lyman-α measurements may lead to a more definitive conclusion about the true solar Lyman-α irradiance value.

3.3 Temporal Calibration

The temporal calibration for the ASSI uses the same data selection criteria as described earlier plus an additional selection based on solar pointing. As discussed by *Tobiska et al.*, [1994], the solar pointing system which corrected for the semiannual 23° change in the solar inclination relative to the ASSI, did not always accurately align the sun to the center of the spectrometer optical axis. When the solar data set are examined as a function of pointing offset, it is found that those data with pointing offsets greater than 3° begin to diverge by more than 10% from the values at the center of the optical axis. For

calculation of the calibration parameters, only data with pointing offsets less than 2.5° are used.

For the temporal calibrations, the brighter solar emission features in each usable ASSI spectrum are extracted using the November 10 calibration parameters. The irradiance for these emissions are then divided by their corresponding values on November 10 and divided by an estimate of their solar variability. These ratios represent the time dependent sensitivity of each channel with respect to their Nov. 10 sensitivity. The solar variability model is based on the *Hinteregger et al.* [1981] proxy model and uses Lyman-α taken from the SME data set as the index for chromospheric emissions, and the F10.7 cm solar radio flux as the index for coronal emissions.

The use of solar proxy models to determine the temporal calibration is unforunately necessary. Our attempts to derive the ASSI temporal calibrations without the use of a solar proxy model, such as empirically determining the solar variability from the ASSI data over a few 27 day solar rotatations, were unsuccessful due mostly to the lack of ASSI data on a daily basis and the fairly large uncertainties for the ASSI measurements. Additionally, there are no other solar EUV spectral irradiance measurements during the earlier period of the San Marco mission that can be used to determine ASSI sensitivity changes during the mission. With the adoption of a proxy model to describe the solar variability, the long-term solar variability from the ASSI measurements will of course agree with the proxy model predictions. However, short-term variability, such as the 27 day solar rotation, could be different between the ASSI measurements and the proxy model. Because the short-term variability for the ASSI measurements agrees well with that predicted from the proxy model at most wavelengths, we believe the solar proxy model presented in the next section is at present the best possible solution for determining the ASSI temporal calibration parameters.

3.3.1 Solar Variability Model

The Hinteregger model is defined by:

$$\frac{F(\lambda,t)}{F(\lambda,t_0)} = V(\lambda,t) = 1 + (R_i(t)-1)\, C(\lambda,t_0), \qquad (1)$$

where $\frac{F(\lambda,t)}{F(\lambda,t_0)}$ is the solar flux ratio of an emission at time t to its value at time t_0 or at the minimum of SC21. R_i is a solar variability index where i=1 refers to chromosperic emissions and i=2 refers to coronal emissions. $C(\lambda,t_0)$ is the contrast ratio given in the AE-E data set SC21refw and describes the variability of an emission with respect to R_i.

Originally, R_1 was defined as the flux ratio of Lyman-β (102.6 nm) to its SC21 minimum value and R_2 was defined as the flux ratio of FE XV (33.5 nm) to its SC21 minimum value. However, these definitions cannot be used for all times because the AE-E dataset only has solar data through the year 1981. R_i has been modeled for all times using the Ottawa 10.7 cm radio flux (F10.7), but because of the large variability of F10.7 we feel that a better model for defining the ASSI temporal calibration for chromospheric emissions should incorporate SME Lyman-α as a solar variability index as follows:

$$V_1(\lambda,t) = 1 + (R_1(t)-1)\frac{C(\lambda,t_1)}{C(Ly\text{-}\alpha,t_1)}, \qquad (2)$$

where $V_1(\lambda,t)$ is the estimated solar variability, $R_1(t)$ is the ratio of SME Lyman-α to its value on November 10 as a function of time, $C(\lambda,t_1)$ is the contrast ratio for each emission feature, and $C(Ly\text{-}\alpha,t_1)$ is the contrast ratio for Lyman-α. The t_1 variable refers to November 10, 1988 as the reference time instead of the SC21 minimum. As stated earlier, we expect the calibration for SME Lyman-α to be different in order to reflect the larger SOLSTICE Lyman-α measurements. However, the R_1 index is a relative value and remains a useful index of chromospheric activity.

The coronal solar variability model uses:

$$V_2(\lambda,t) = 1 + (R_2(t)-1)C(\lambda,t_1), \qquad (3)$$

where R_2 is normalized to unity on November 10 (F10.7 = 152.4, <F10.7> = 166.7) and is estimated by using the F10.7 index :

$$R_2 = A\langle F10.7\rangle + B[F10.7 - \langle F10.7\rangle] + C, \qquad (4)$$

with A = 0.0125, B = 0.00729, C = -0.976, and <F10.7> is the 81 day average of F10.7. In Figure 4 are plots of the Ottawa 10.7 cm solar flux and SME Lyman-α indices for the year 1988.

Because the reference spectrum used to define R_1 and R_2 in this paper is different from the solar minimum reference spectrum used by Hinteregger, the contrast ratios in equations 1 and 2 must be revised from the Hinteregger contrast ratios. The Hinteregger model uses a linear relationship to compare the solar irradiance at one wavelength to the solar irradiance at different wavelengths,

$$F(\lambda,t) = A + B\, F_{ref}(\lambda',t)\,, \qquad (5)$$

where F is the modeled emission, F_{ref} is the measured reference emission, and A and B are the linear fit coefficients.

From equation 1 or 2, the Hinteregger model defines $V(\lambda,t)$ as $\frac{F(\lambda,t)}{F(\lambda,t_0)}$, where $F(\lambda,t_0)$ is the irradiance of an emission at some reference time t_0. Replacing $V(\lambda,t)$ by $\frac{F(\lambda,t)}{F(\lambda,t_0)}$ and R by $\frac{F_{ref}(\lambda',t)}{F_{ref}(\lambda',t_0)}$ in equation 1 or 2 gives:

$$F(\lambda,t) = F(\lambda,t_0)\,(1 - C(\lambda)) + C(\lambda)\,F(\lambda,t_0)\,\frac{F_{ref}(\lambda',t)}{F_{ref}(\lambda',t_0)}. \qquad (6)$$

Identifying $F(\lambda,t_0)\,(1 - C(\lambda))$ as the coefficient A in equation 4 and $\frac{C(\lambda)F(\lambda',t_0)}{F_{ref}(\lambda',t_0)}$ as the coefficient B, equation 5 must give the same solution for every reference spectrum because $F(\lambda,t)$ and $F_{ref}(\lambda',t)$ are absolutely measured values. Therefore, for two reference irradiances measured at times t_0 and t_1,

$$F(\lambda,t_0)\,(1 - C(\lambda,t_0)) = F(\lambda,t_1)\,(1 - C(\lambda,t_1)) \text{ or,} \qquad (7a)$$

$$C(\lambda,t_1) = 1 - \frac{F(\lambda,t_0)\,(1 - C(\lambda,t_0))}{F(\lambda,t_1)} \qquad (7b)$$

Using t_0 as the reference time of the SC21 minimum and t_1 as the ASSI reference time of Nov. 10, the ASSI contrast ratios must be redefined from the Hinteregger contrast ratios. Using the standard form of the Hinteregger model from eqn. 1,

$$F(\lambda,t) = F(\lambda,t_0)(1 + (R_i(t) - 1)\,C(\lambda,t_0))\,, \qquad (8)$$

equation 7 can be re-written as:

$$C(\lambda,t_1) = 1 - \frac{1 - C(\lambda,t_0)}{1 + (R_i(t_1) - 1)C(\lambda,t_0)} \qquad (9)$$

Because the time period for the AE-E dataset did not overlap with the ASSI mission, we must use the estimated value of R_i which uses F10.7 as an index:

$$R_i = A\langle F10.7\rangle + B(F10.7 - \langle F10.7\rangle) + C. \qquad (10)$$

where R_i is normalized to unity during the minimum of SC21. A = 0.0113, B = 0.0049 and C = 0.496 for chromospheric emissions giving R_1 a value of 2.3 on November 10, 1988. A = .625, B = .365, and C = -48.9 for coronal emissions giving R_2 a value of 50.1 on November 10, 1988. The modified contrast ratios as derived from equation 9 are the appropriate values for equations 2 and 3. The Hinteregger contrast ratios and the November 10, 1988 contrast ratios calculated with equations 9 and 10 are listed in Table 2.

3.3.2 Sensitivity Change Model

It is found from the sensitivity ratios that exponential curves can describe the sensitivity changes of the ASSI optics and detectors. We have identified mechanisms for both increasing and decreasing instrument sensitivities. To increase sensitivity, previously deposited contaminants are removed from the optics by either evaporation in the space environment or scrubbing by solar radiation. To decrease sensitivity, particulate contaminants, which most likely have lower efficiencies to UV photons, are deposited on the optics during the mission. The polymerization of these contaminants into a film by solar radiation may also cause the efficiency to drop dramatically. The most likely sources of these contaminants are hydrocarbons from a vacuum accident involving the ASSI A module prior to the mission, and spacecraft outgassing from prolonged vacuum exposure during the mission. A model that incorporates these processes follows.

The quantum throughput or sensitivity of an instrument at some instance in time is defined by:

$$S = \frac{A_{tot} - A_c}{A_{tot}} S_o + \frac{A_c}{A_{tot}} S_c = S_o + \frac{A_c}{A_{tot}} (S_c - S_o). \qquad (11)$$

where S is the total sensitivity of the instrument, S_o and S_c are the uncontaminated and contaminated sensitivities, A_c is the contaminated surface area and A_{tot} is the total surface area. We expect that contaminants absorb most UV photons such that $S_c << S_o$; therefore,

$$S \approx S_o(1 - \frac{A_c}{A_{tot}}). \qquad (12)$$

The total area covered by the contaminants are:

$$A_c = N_p A_p + N_f A_f + N_g A_g \tag{13}$$

where N_p refers to pre-existing particulate contaminants such as those released during the ASSI A vacuum accident, N_f is the number of polymerized contaminant films and N_g is the number of particulates resulting from spacecraft outgassing. A_p, A_f and A_g are their respective average surface areas.

Possible rate equations for N_p, N_f and N_g are

$$\frac{dN_p}{dt} = -(k_f + k_r)N_p = -k\,N_p, \tag{14a}$$

$$\frac{dN_f}{dt} = k_f N_p = -\frac{k_f}{k}\frac{dN_p}{dt}, \tag{14b}$$

$$\frac{dN_g}{dt} = R_g e^{-k_g t}, \tag{14c}$$

where k_f and k_r are the rate constants for creating a film out of a particle and removing a particle respectively. R_g is the initial deposition rate for spacecraft outgassing and k_g describes how the deposition rate changes with time. Integrating equations 14 gives

$$N_p = N_o e^{-k(t - t_0)}, \tag{15a}$$

$$N_f = -\frac{k_f}{k} N_o e^{-k(t - t_0)} + \frac{k_f}{k} N_o, \tag{15b}$$

$$N_g = \frac{R_g}{k_g}(1 - e^{-k_g(t - t_0)}). \tag{15c}$$

Inserting equations 15 into equation 13 results in

$$A_c = A_p N_o e^{-k(t - t_0)} + A_f \frac{k_f}{k} N_o(1 - e^{-k(t - t_0)}) + A_g \frac{R_g}{k_g}(1 - e^{-k_g(t - t_0)}). \tag{16}$$

Placing equation 15 into equation 11 and combining all the constants together yields:

$$\frac{S}{S_o} = A + B\, e^{-k\,(t - t_0)} + C\, e^{-k_g\,(t - t_0)} \qquad (17)$$

where the constants A and B can take positive or negative values and the constant C can only be positive. This model can include the effects of other contaminants by adding more exponential terms to equation 17. The sensitivity ratios as a function of time for emissions from channels 11 and 18 from ASSI A are presented in Figure 5 with possible fits to these ratios using equation 16. These time series indicate that both increases or decreases in detector sensitivity are possible.

The ASSI A channels show sensitivities that increase with time during the early part of the mission followed by a decrease; this behavior is consistent with the dual contaminant model and could result from the simultaneous removal of the pre-flight hydrocarbon contaminants from the detector and optics surfaces and contaminant deposition from spacecraft outgassing on the detectors surfaces. Although equation 16 can describe the ASSI sensitivity changes over the entire mission, a simpler form of equation 16, a single exponential term, is also acceptable for the ASSI EUV channels as described next.

3.3.3 ASSI Sensitivity Changes

It is found that the ASSI sensitivity rate of change differs at the beginning and end of the mission for some wavelengths. These changes correspond to spin-adjust maneuvers by the San Marco satellite between days 202 and 262 of the year 1988. These maneuvers appear to have changed the ASSI sensitivities, possibly by illuminating different regions of the ASSI optics. There were very few solar measurements during these maneuvers, and it was therefore difficult to analyze the sensitivity changes of this time period. For this reason, the temporal calibration of the ASSI is derived by fitting single exponential curves to the sensitivity ratios for the time periods before day 203 and after day 262. The exponential lifetime parameters from these fits are inverted to describe the expected fractional change in sensitivity from day 100 to day 315 (Nov 10) of 1988 as follows.

$$f_i(\lambda) = 1 - \exp\left(\frac{-\Delta T}{\tau_i(\lambda)}\right), \qquad (18)$$

where $i = 1$ indicates the time period before day 203 and $i = 2$ indicates the time period after day 262. The τ is the lifetime parameter and $\Delta T = 215$ and is an arbitrary constant representing the mission lifetime. These functions are used to determine the temporal

calibration because they are much smoother between wavelengths than exponential lifetimes and can be easily interpolated to all wavelengths by using a fourth order polynomial. The sensitivity change between days 203 and 262 is derived by matching a third function f_3 to the ending value of f_1 and the beginning value of f_2.

$$f_3(\lambda,t) = \frac{1}{60}[\,(262 - t)\, f_1(\lambda) + (t - 202)\, f_2(\lambda))], \qquad (19)$$

where "t" is a day of the year 1988. Table 3 lists the polynomial coefficients for computing f_1 and f_2.

The absolute solar irradiance or terrestrial airglow can be obtained by applying the November 10 calibration parameters to the raw count rate and then factoring the resultant flux by $\exp(\frac{315-t}{\tau_i(\lambda,t)})$ as the temporal calibration correction. The τ_i can be derived by inverting equation 17 to give:

$$\tau_i = \frac{-215}{\ln(1 - f_i)}, \qquad (19)$$

where again i = 1,2 or 3 to represent the different mission time periods. The sensitivities with respect to November 10, 1988 for the EUV channels are presented in Figure 6 as a function of time and wavelength.

4.0 ASSI Data Quality

In general, the results from the photometric calibration procedure yield good agreement of the EUV solar irradiance for the overlap regions between channels. The best agreements are at wavelengths where the statistical uncertainty in the count rate is greater than 10% and where the count rates are much higher than background counts. The precision for the ASSI solar measurements is much larger than the desirable 1% value needed for accurate solar variability analysis because the ASSI operation, coupled with the spinning satellite, only permitted an integration period of less than a second per wavelength. Solar emission features with good counting statistics are at 58.4 nm (He I), 61.0 nm (Mg X), 63.0 nm (O V), 77.0 nm (Ne VIII), 79.0 nm (O IV), 80 nm through 90 nm (H I, O III, O II), 83.4 nm (O III, O II), 97.7 nm (C III), 102.5 nm (H Ly-β) and 121.5 nm (H Ly-α).

Those emissions with poor counting statistics or high background counts have daily variations that do not agree well with the 13 and 27 day solar rotation variability, and their irradiances do not usually agree well in the overlap regions between channels. Plots of the November 10 raw count rates of each of the EUV channels 12, 16, and 18 are presented in

Figure 7. A count rate of 400 counts/sec corresponds to a counting uncertainty of 10% as the ASSI detector integration period is .25 seconds. Time series of two solar emission features that are measured by multiple channels are shown in Figure 8. The top panel of Figure 8 shows the time series irradiance for the 70.3 nm O III emission measured by channels 12, 16 and 18. As shown in Figure 7, this emission has low counting statistics relative to the background counts which confirms the poor agreement between channels. A similar plot is shown in the bottom panel of Figure 8 of the hydrogen continuum between 85 and 90 nm. This wavelength region has good counting statistics in channels 12, 16 and 18, and the agreement between channels is significantly improved.

5.0 Discussion of ASSI Solar Measurements

Solar emission features extracted from the ASSI are compared to their predicted irradiance from the *Hinteregger* [1981] and EUV91 [*Tobiska*, 1991] models in Table 4. Like the solar variability model presented earlier, the daily modeled irradiance for each solar emission is normalized to its November 10 value. These emission ratios are then multiplied by their respective reference irradiances given by *Schmidtke et al.* [1992]. These normalized irradiances have a higher correlation with their values measured by the ASSI than the absolute irradiance predicted by these two models because both models are based on different reference spectra. The ratio of the ASSI's measured irradiance on November 10 to the models absolute irradiance are included in Table 4. These comparisons of absolute irradiances suggest refinements for the proxy models' reference spectra with factors as much as 2 needed.

Because of the modest spectral resolution of ASSI, many of the emission lines are blended and cannot be extracted from the spectra and analyzed separately. As discussed earlier, lines are not tabulated if there were too few measurements or if the counting statistics were too poor to provide a meaningful data set. As seen in Table 4, the agreement between the modeled and measured irradiance for each solar emission feature is best for emission features whose counting statistics are good. Those solar emissions with good counting statistics, as identified in Figure 7, are at wavelengths of 58.4 nm, 61.0 nm, 63.0, 77.0 nm, 79.0 nm, 80 to 90 nm, 97.7 nm, 102.5 nm, and 121.5 nm. The time series irradiance for these emission features, except for Lyman-α at 121.5 nm, are presented in Figures 9 through 11 along with the irradiance predictions from the Hinteregger and the EUV91 models which have been normalized to produce the Nov. 10 ASSI reference spectra. Good overall agreement over the mission lifetime is expected

between the modeled and measured irradiances because the Hinteregger model defined in this paper is used to determine the temporal calibration parameters. We attempted to analyse the 27 day modulation of each emission's time series by dividing the time series by their respective modeled 81 day average. Unfortunately, this analysis gave poor correlation coefficients, .1 to .5, between the measured and modeled 27 day modulation for all of the ASSI EUV emissions, probably because there were no daily measurements over several 27 day solar rotatiions. We also attribute the poor correlation to the fact that the combined precision of the ASSI EUV measurements and SME Lyman-a was of the same magnitude as the average 27 day variability with respect to the local mean intensity during 1988. However, Figures 9 through 11 do show the range of variability expected from solar EUV emissions. The 27 day solar variability for the emissions at 61.0 nm (Mg X), 63.0 nm (O V), 80 - 90 nm (Hydrogen continuum), and 102.5 nm (Lyman-β) appear to be consistent with the modeled variability, whereas the time series for the 58.4 nm (He I), 77.0 nm (Ne VIII), 79.0 nm (O IV), and 97.7 nm (C III) emissions reveal that the 27 day solar variability of these emissions appear larger than the model's predictions. It is uncertain how this result would affect the Hinteregger contrast ratios because there may be intrinsic differences between short term and long term solar variability and because the ASSI data quality is not precise enough to warrant adjusting the contrast ratios.

The percentage increases for extractable solar EUV emission lines between day 119 of the ASSI mission and days 160 and 315 are presented in Table 5. The solar variability between days 119 and 315 show the range in solar variability over the ASSI mission. As can be seen from Figure 4, day 119 is a minimum in the 27 day solar rotation modulation of SME Lyman-α and the 10.7 cm solar radio flux whereas day 160 is a maximum of the 27 day modulation. We find that the variability of the lower temperature coronal lines 61.0 nm (Mg X) and 77.0 nm (Ne VIII) have variabilities of approximately 40% and 61% respectively between the minimum and maximum of the 27 day solar rotation . These values can be compared to the variability of the other emissions in Table 5 originating in the solar transition region and chromosphere which vary between 10% and 30% over the same time period. The ASSI calibration changes between days 119 and 160 are small enough such that the measured 27 day solar variability of these emissions in this period should be approximately correct.

6.0 Summary

The ASSI optics and detectors exhibit sensitivity changes that can be characterized by exponential curves. A sensitivity change model, that incorporates scrubbing of

contaminants, contaminant polymerization and spacecraft outgassing onto the optics, is consistent with the expected ASSI sensitivity changes which show both increases and degradation of the sensitivity. The ASSI calibration parameters for channels 12,16 and 18 have approximately a 20% uncertainty for solar EUV measurements. The solar calibration is directly applicable for the ASSI terrestrial airglow measurements but with a slightly larger uncertainty of about 30%.

The ASSI measurement of solar Lyman-α on Nov. 10 1988 is found to be 5.8×10^{11} photons s^{-1} cm^{-2} with an uncertainty of 20%. This value is much larger than the SME solar Lyman-α measurement of 3.35×10^{11} photons s^{-1} cm^{-2} but is in agreement with the value of 5.8×10^{11} photons s^{-1} cm^{-2} that is predicted from the UARS SOLSTICE Lyman-α measurements for time periods of similar solar activity.

The absolute solar EUV irradiances predicted by the Hinteregger and EUV91 models have systematic differences with the solar irradiance measured by the ASSI. These differences are likely related to photometric calibration differences between earlier measurements, namely AE-E and the ASSI measurements. It is found that the 27 day solar rotation variability for emissions at 58.4 nm (He I), 77.0 nm (Ne VIII), 79.0 nm (O IV), and 97.7 nm (C III) are larger than the 27 day variability predicted from the Hinteregger and EUV91 models, whereas the 27 day solar variability of emissions at 61.0 nm (Mg X), 63.0 nm (O V), 80 - 90 nm (Hydrogen Continuum), and 102.5 nm (Lyman-β) are in good agreement with the Hinteregger and EUV91 models. These results from the ASSI solar data suggest that the intensity of the proxy models needs to be adjusted, but there was not enough solar data to warrant specific changes in the Hinteregger contrast ratios.

References

Conway, R. R., Photoabsorption and photoionization cross sections of O, O_2 and N_2 for photoelectron production calculations: a compilation of recent laboratory measurements, *NRL Memorandum Report 6155*, Naval Research Laboratory, Washington, DC, 1988.

Fennelly, J. A. and D. G. Torr, Photoionization and photoabsorption cross section of O, N_2, O_2 for aeronomic calculations, *Atomic Data and Nuclear Data Tables, 51*, 321, 1992.

Hedin, A. E., MSIS-86 thermospheric model. *J. Geophys. Res. 92*, 4649, 1987

Hintergger, H. E., K. Fukui, and B.R. Gilson, Observational, reference and model data on solar EUV from measurements on AE-E, *Geophys. Res. Letters, 8*, 1147, 1981.

Hoegy, W. R., W. D. Pesnell, T. N. Woods, and G. J. Rottman, How active was solar cycle 22, *Geophys. Res. Lett., 20*, 1335, 1993.

Rottman, G.J., T.N. Woods, and T.P. Sparn, Solar-Stellar Comparison Experiment, 1, 1, Instrument Design and Operation, *J. Geophys Res. 98*, 10667, 1993.

Schmidtke, G., P. Seidl, and C. Wita, Airglow-solar spectrometer instrument (20-700 nm) aboard the San Marco D satellite, *Applied Optics,24*, 3206, 1985

Schmidtke, G., T.N. Woods, J. Worden, G.J. Rottman, H. Doll, C. Wita, S.C. Soloman, Solar EUV irradiance from the San Marco ASSI: A reference spectrum, *Geophys. Res. Letters, 19*, 2175, 1992.

Tobiska, W.K., G. Schmidtke, H. Doll, T. Woods, J. Worden, S. Chakrabarti, Comparison of San Marco ASSI solar EUV and EUV91 model, *COSPAR Colloquium No. 5, (in press)*1994.

Tobiska, W.K., Revised solar extreme ultraviolet flux model, *J. of Atmospheric and Terrestrial Physics, 53*, 1005, 1991.

Woods, T.N. and G.J. Rottman, Solar EUV irradiance derived from a sounding rocket experiment on 10 November 1988, *J. Geophys. Res. 95*, 6227, 1990.

Woods, T.N., G.J. Rottman, and G.J. Ucker, Solar Stellar Irradiance Experiment, 1, 2, Instrument Calibration, *J. Geophys Res. 98*, 10,679, 1993.

TABLE 1. Spectral resolution and wavelength ranges of the ASSI EUV channels

Channel	Resolution (nm)	Wavelength Range (nm)
12	1.22	50.0 - 97.3
16	.82	55.3 - 110.1
18	1.22	57.4 - 139.0

TABLE 2. The Hinteregger and revised contrast ratios.

Wavelength (nm)	Ion	Class	Hinteregger Contrast Ratio	Nov. 10 Contrast Ratio
58.4	He I	1	0.998	0.995
61.0	Mg X	2	0.0280	0.591
63.0	O V	1	0.473	0.674
70.3	O III	1	0.415	0.620
77.0	Ne VIII	2	0.0220	0.530
79.0	O IV	1	0.460	0.662
80 - 85	H I,OII,OII	1	0.796	0.900
83.4	O II, OIII	1	0.415	0.620
85-90	H I continuum	1	1.00	1.00
95.0	H I Ly-δ	1	1.00	1.00
97.7	C III	1	0.608	0.781
102.5	H I Ly-β	1	1.00	1.00
108.5	N II	1	0.498	0.695
121.5	H I Ly-α	1	0.830	0.918
130.4	O I	1	0.415	0.620

The Hinteregger contrast ratios are taken from the AE-E data set SC21REFW. Class 1 is for chromospheric emissions and class 2 is for coronal emissions. The ASSI contrast ratios are calculated using equations 8 and 9 for use with the Nov. 10 reference spectra.

TABLE 3. Polynomial coefficients for f_1 and f_2

Channel	Function	Polynomial Coefficients				
		λ^0	λ^1	λ^2	λ^3	λ^4
12	f_1	0.05280	0.04665	-0.001895	2.506×10^{-5}	-1.06×10^{-7}
12	f_2	-2.393	0.1968	-0.006713	8.712×10^{-5}	-3.70×10^{-7}
16	f_1	-9.440	0.5637	-0.0121	1.123×10^{-4}	-3.79×10^{-7}
16	f_2	0.6180	-0.00783	-0.00059	1.31×10^{-5}	-6.70×10^{-8}
18	f_1	0.09020	-0.02105	5.026×10^{-4}	-2.81×10^{-6}	5.1×10^{-10}
18	f_2	-6.406	0.3443	-0.006382	5.019×10^{-5}	-1.41×10^{-7}

The fractional change of sensitivity, f_1 and f_2 are described by equation 17. Each f is given by $f = \sum A_i \lambda^i$, where λ is given in nanometers. The coefficients A_i are given below for each power of λ.

TABLE 4. Comparison of Measured and Modeled Solar Irradiance

Wavelength (nm)	Ion	ASSI Channels	Variability Differences		Absolute Flux Ratio	
			Hinteregger	EUV91	Hinteregger	EUV91
58.4	He I	12,16,18	0.16	0.13	1.36	1.91
61.0	Mg X	12,16,18	0.18	0.18	0.938	1.11
63.0	O V	12,16,18	0.11	0.12	1.46	1.01
77.0	Ne VIII	12,16,18	0.40	0.39	0.991	1.25
79.0	O IV	12,16,18	0.18	0.17	0.380	1.12
80 - 85	H I,OII,OII	12,16,18	0.098	0.077	0.384	0.639
83.4	O II, OIII	12,16,18	0.088	–	1.44	–
85-90	H I cont.	12,16,18	0.087	0.080	0.481	0.867
95.0	H I Ly-δ	16	0.12	0.14	0.983	–
97.7	C III	16,18	0.13	0.096	0.856	1.06
102.5	H I Ly-β	16,18	0.070	0.075	0.942	1.13
121.5	H I Ly-α	18	0.073	–	1.00	–

The variability differences are the RMS differences between the ASSI measurement and the *Hinteregger* [1981] and EUV91 [*Tobiska*, 1991] models. The ratio of the absolute flux from ASSI to model predictions is for November 10, 1988. A dash indicates that there exist no predictions from the EUV91 model at these specific wavelengths.

TABLE 5. Solar variability for ASSI solar EUV emissions.

Wavelength (nm)	Ion	Percent Increase in Solar Irradiance	
		Days 119 - 160	Days 119 - 315
58.4	He I	27	10
61.0	Mg X	40	43
63.0	O V	22	20
77.0	Ne VIII	61	5
79.0	O IV	15	20
80 - 85	H I,OII,OIII	25	25
83.4	O II, OIII	22	30
85-90	H I continuum	31	33
95.0	H I Ly-δ	38	37
97.7	C III	21	19
102.5	H I Ly-β,OVI	41	34
121.5	H I Ly-α	22	27

Figure Captions

Fig. 1. Calibration parameters for the ASSI EUV channels derived for November 10 1988 using the sounding rocket reference spectrum. Channel 12 (dotted line), channel 16 (large dashes), channel 18 (solid line).

Fig. 2. The EUV channel detector sensitivity change since the pre-flight calibration as measured by radioactive beta sources. Channel 12 (pluses), channel 18 (triangles), channel 16 (diamonds).

Fig. 3. Panel (a): channel 18 pre-flight calibration parameters. Panel (b): channel 18 Nov. 10 calibration normalized to rocket spectra and SME Lyman-α (solid line), and channel 18 Nov. 10 calibration normalized to rocket spectra (dashed line).

Fig. 4. Indices used in the solar variability model for the year 1988. The days when the ASSI had full solar spectral measurements are indicated as the diamond symbols.

Fig. 5. Expected and modeled sensitivity change for emissions at 102.5 nm and 121.5 nm measured by the ASSI A channels 18 and 11 respectively. The equations $\frac{S}{S_0}$ given in each panel is the modeled sensitivity change using equation 16 and is represented by the solid line. The diamonds are the expected sensitivity change.

Fig. 6a. Channel 12 sensitivity normalized to unity on Nov 10 as a function of time and wavelength.

Fig. 6b. Channel 16 sensitivity normalized to unity on Nov 10 as a function of time and wavelength.

Fig. 6c. Channel 18 sensitivity normalized to unity on Nov 10 as a function of time and wavelength.

Fig. 7. Raw count rates for the ASSI EUV channels on November 10, 1988. Dashed line indicates 10% uncertainty in counting statistics as the ASSI count integration time is .25 seconds.

Fig. 8. Comparison among the EUV channels of the ASSI measured irradiance
emissions at 70.3 nm and 85-90 nm . Channel 12 (pluses), channel 16 (diamond
channel 18 (squares).

Fig. 9. Comparison of ASSI solar emissions (diamonds) to the Hinteregger proxy mode
(solid line) and EUV91 proxy model (dashed line) for emissions at 58.4 nm (He I), 61.0
nm (Mg X) and 63.0 nm (O V).

Fig. 10. Comparison of ASSI solar emissions (diamonds) to the Hinteregger proxy model
(solid line) and EUV91 proxy model (dashed line) for emissions at 77.0 nm (Ne VIII)
79.0 nm (O IV) and 80 - 85 nm (Hydrogen continuum, OII, O III)

Fig. 11. Comparison of ASSI solar emissions (diamonds) to the Hinteregger proxy model
(solid line) and EUV91 proxy model (dashed line) for emissons at 85 - 90 nm (Hydrogen
continuum), 97.7 nm (C III) and 102.5 nm (Lyman-β, O VI)

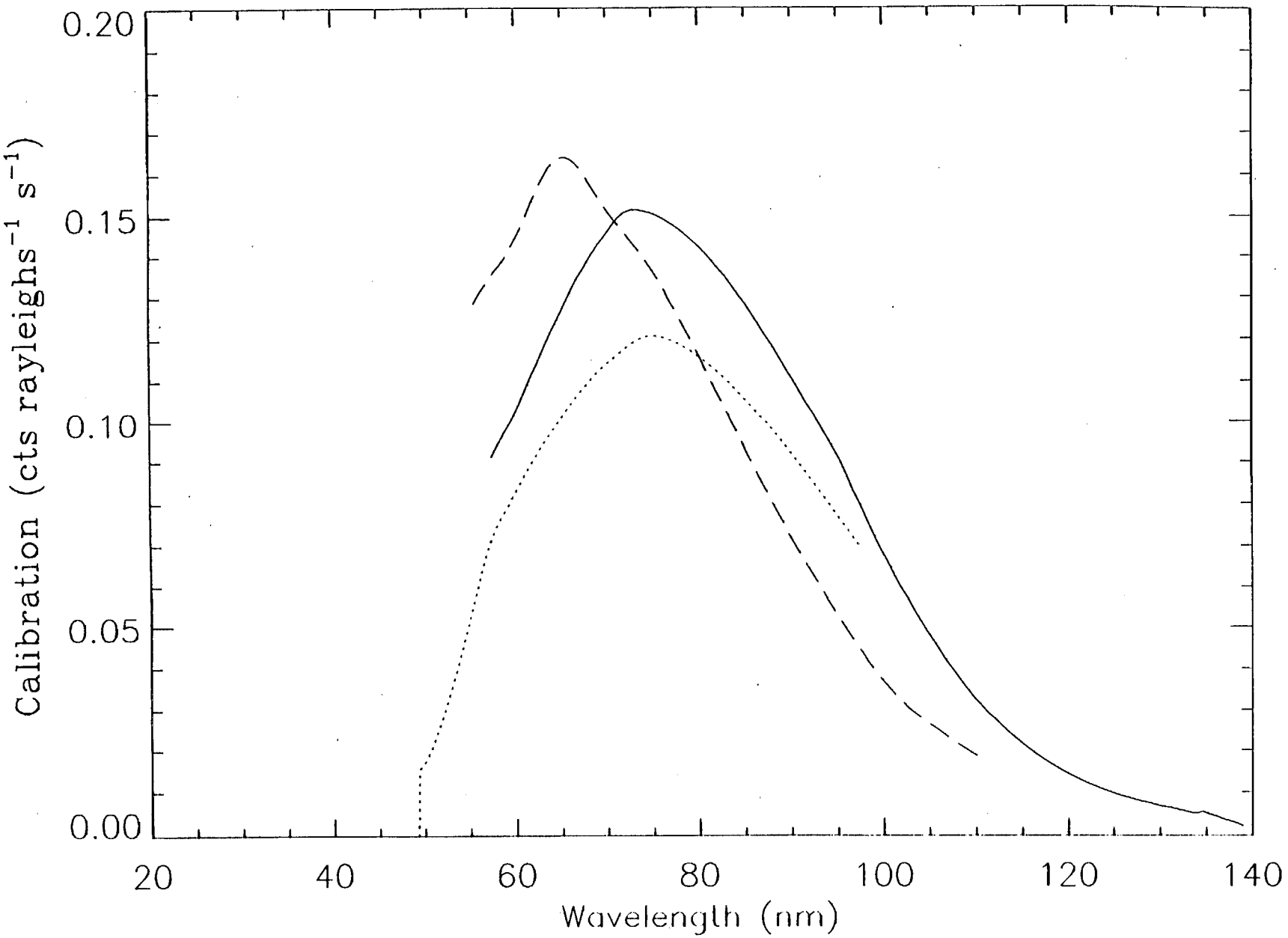
0.20
0.15
0.10
0.05
0.00
Calibration (cts rayleighs^{-1} s^{-1})
20
40
60
80
100
120
140
Wavelength (nm)

Fig 1

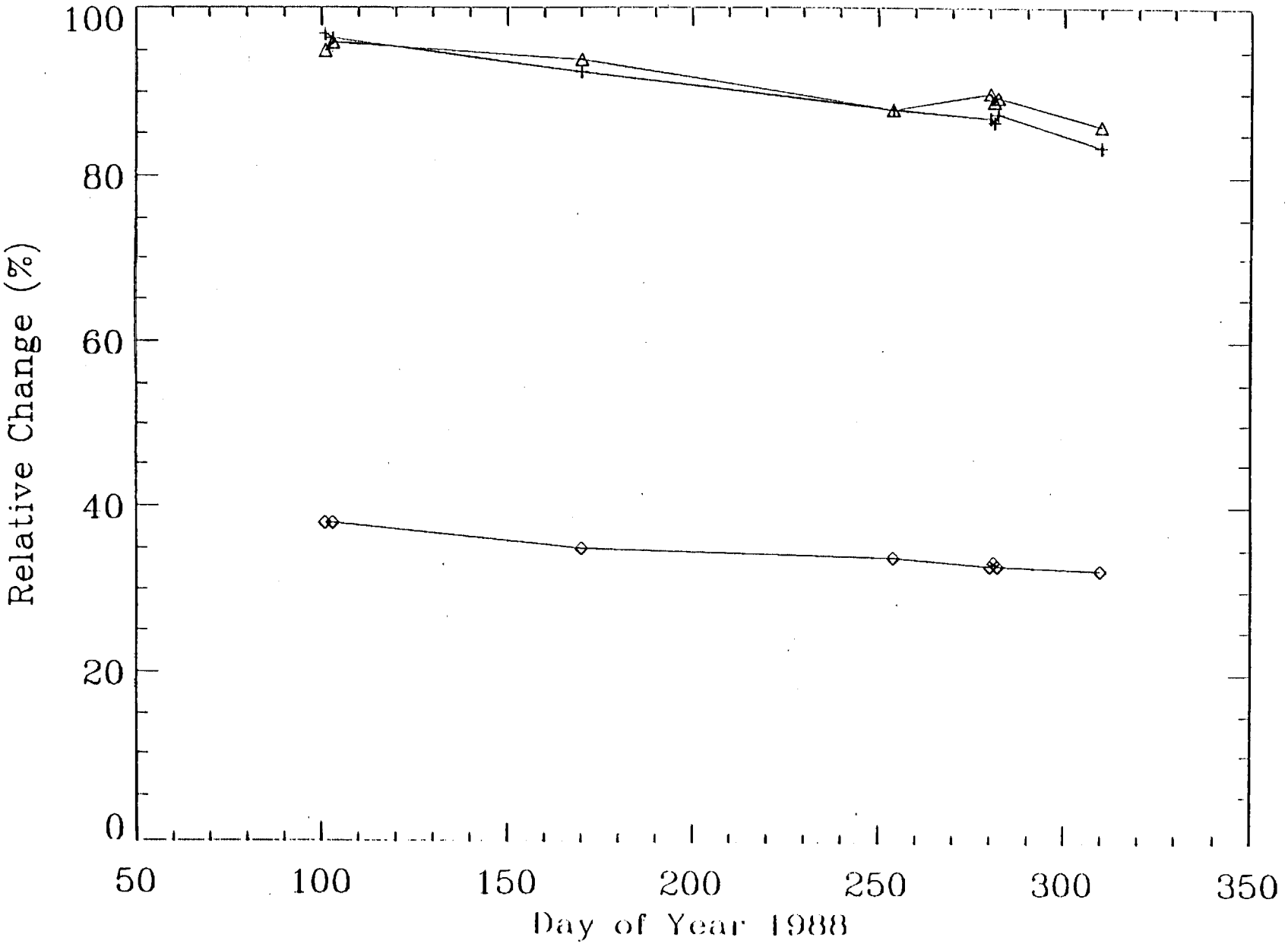
100
80
60
40
20
0
Relative Change (%)
50
100
150
200
250
300
350
Day of Year 1988

Fig 2

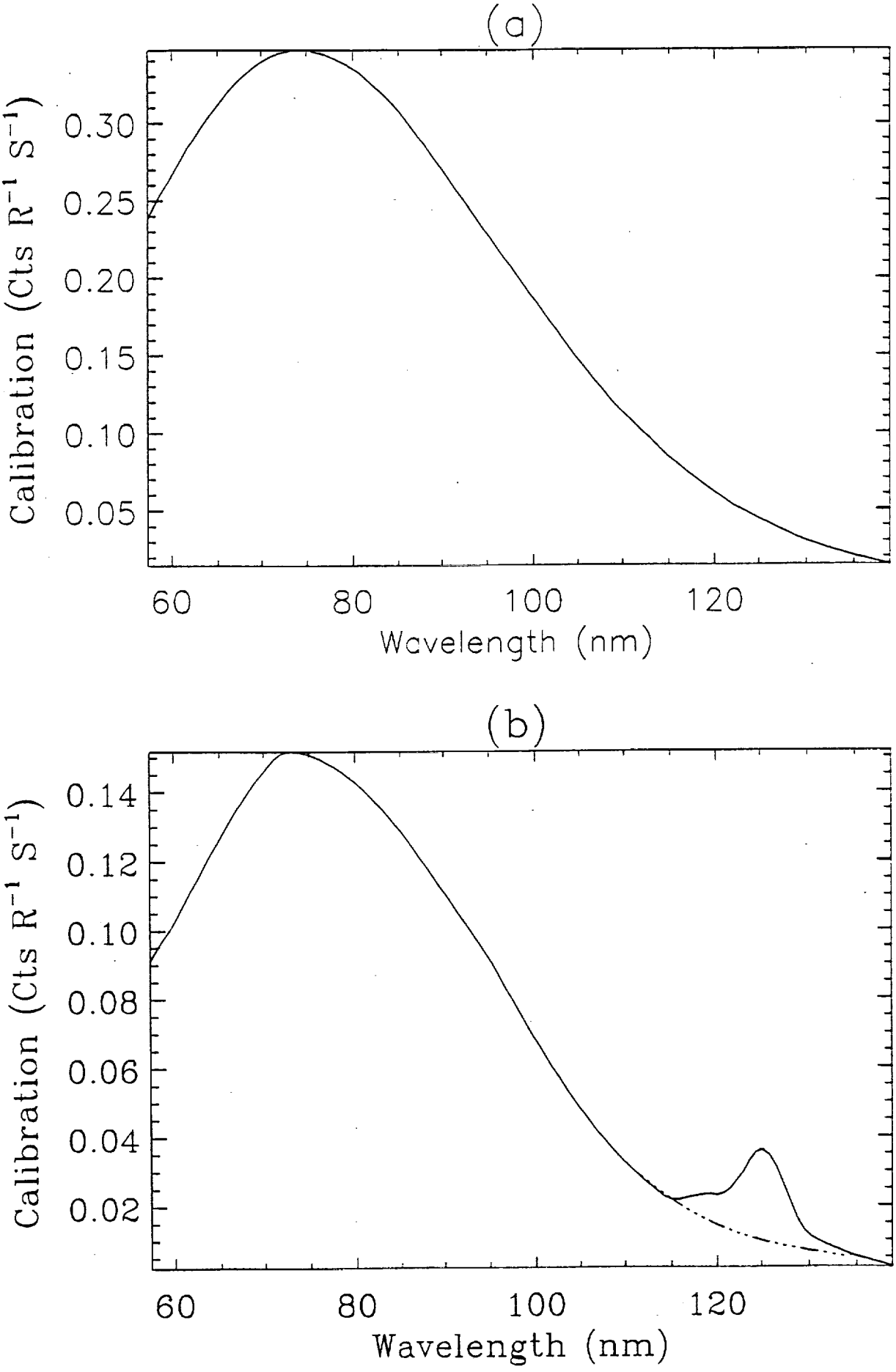
(a)
Calibration (Cts R^{-1} S^{-1})
0.30
0.25
0.20
0.15
0.10
0.05
60
80
100
120
Wavelength (nm)
(b)
Calibration (Cts R^{-1} S^{-1})
0.14
0.12
0.10
0.08
0.06
0.04
0.02
60
80
100
120
Wavelength (nm)

Fig 3

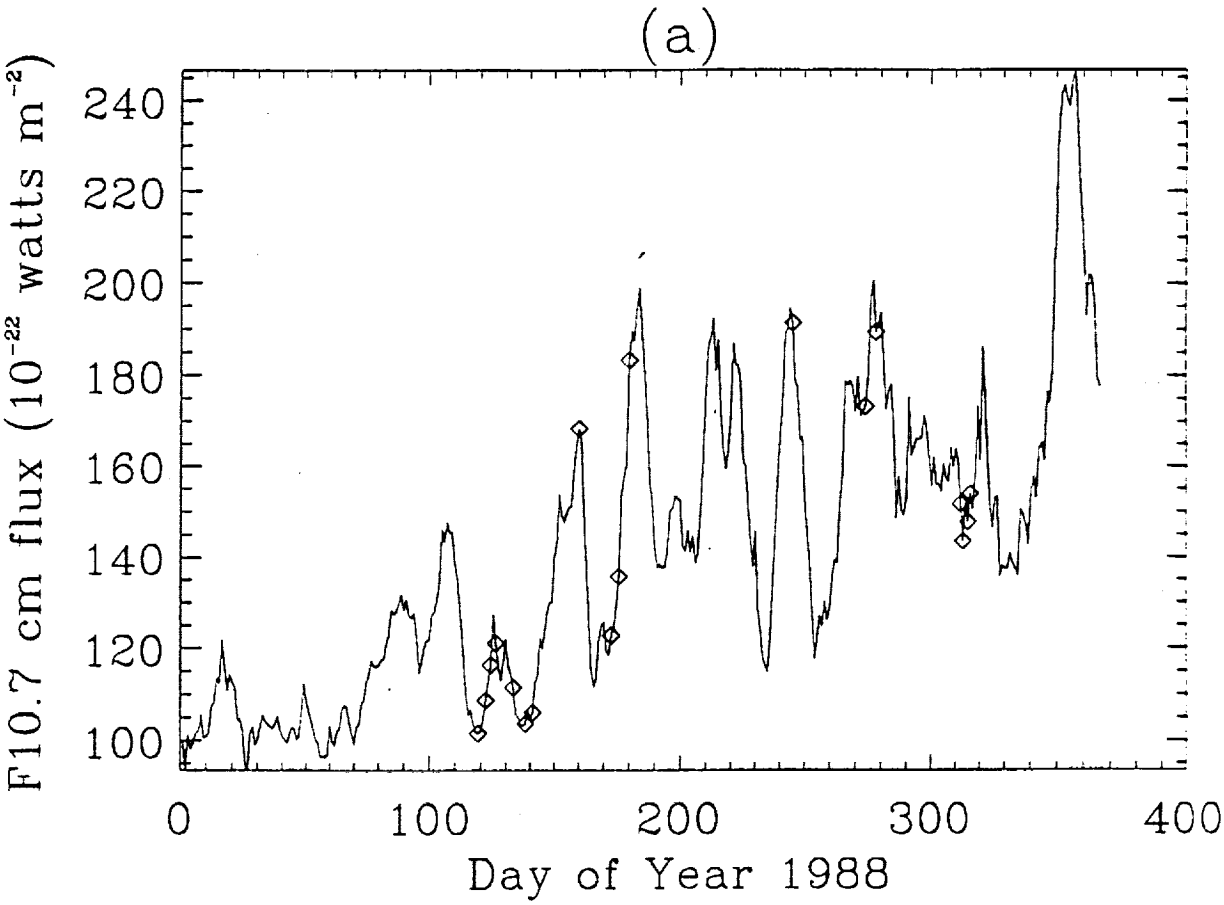
(a)
F10.7 cm flux (10^{-22} watts m^{-2})
240
220
200
180
160
140
120
100
0
100
200
300
400
Day of Year 1988

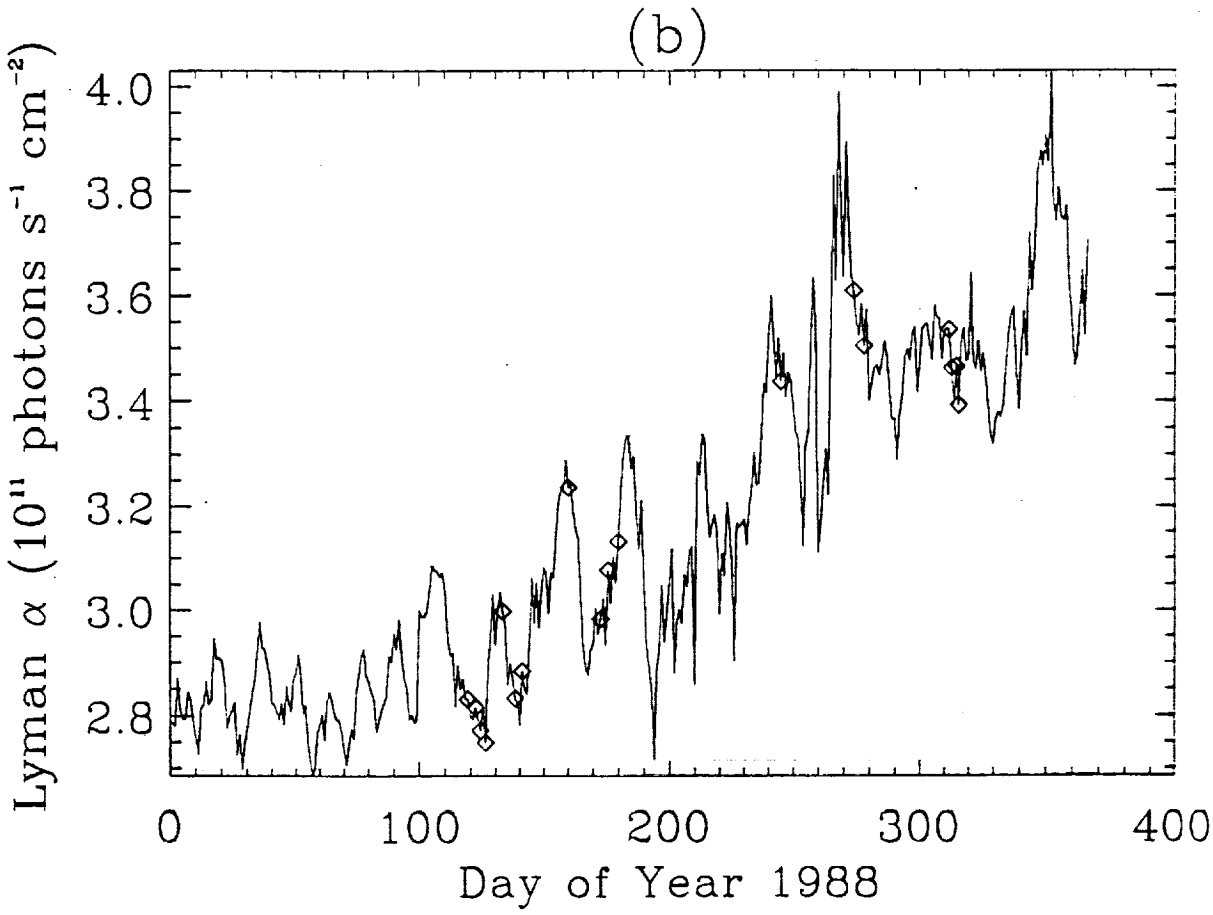
(b)
Lyman α (10^{11} photons s^{-1} cm^{-2})
4.0
3.8
3.6
3.4
3.2
3.0
2.8
0
100
200
300
400
Day of Year 1988

Fig 4

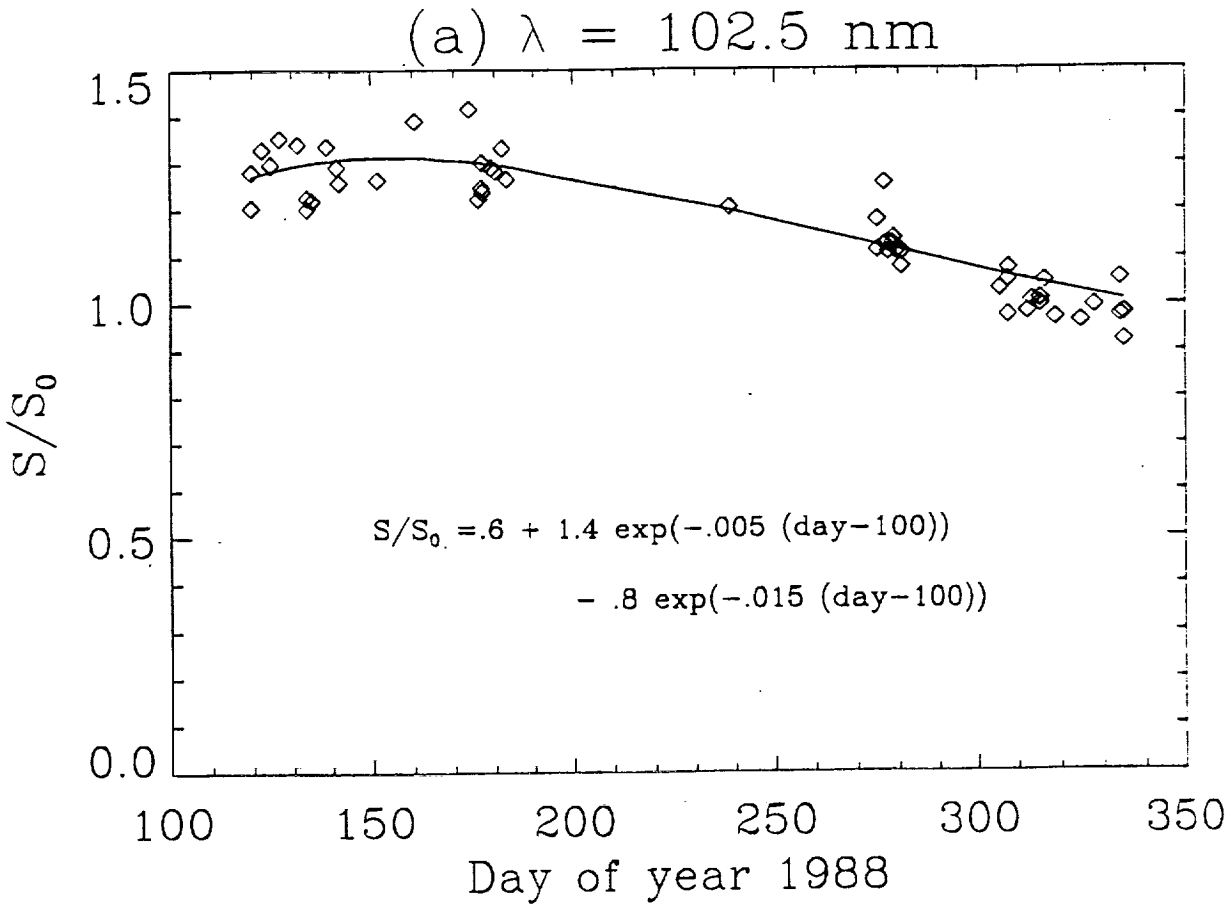
(a) λ = 102.5 nm
1.5
1.0
0.5
0.0
S/S0
S/S0 =.6 + 1.4 exp(−.005 (day−100))
− .8 exp(−.015 (day−100))
100
150
200
250
300
350
Day of year 1988

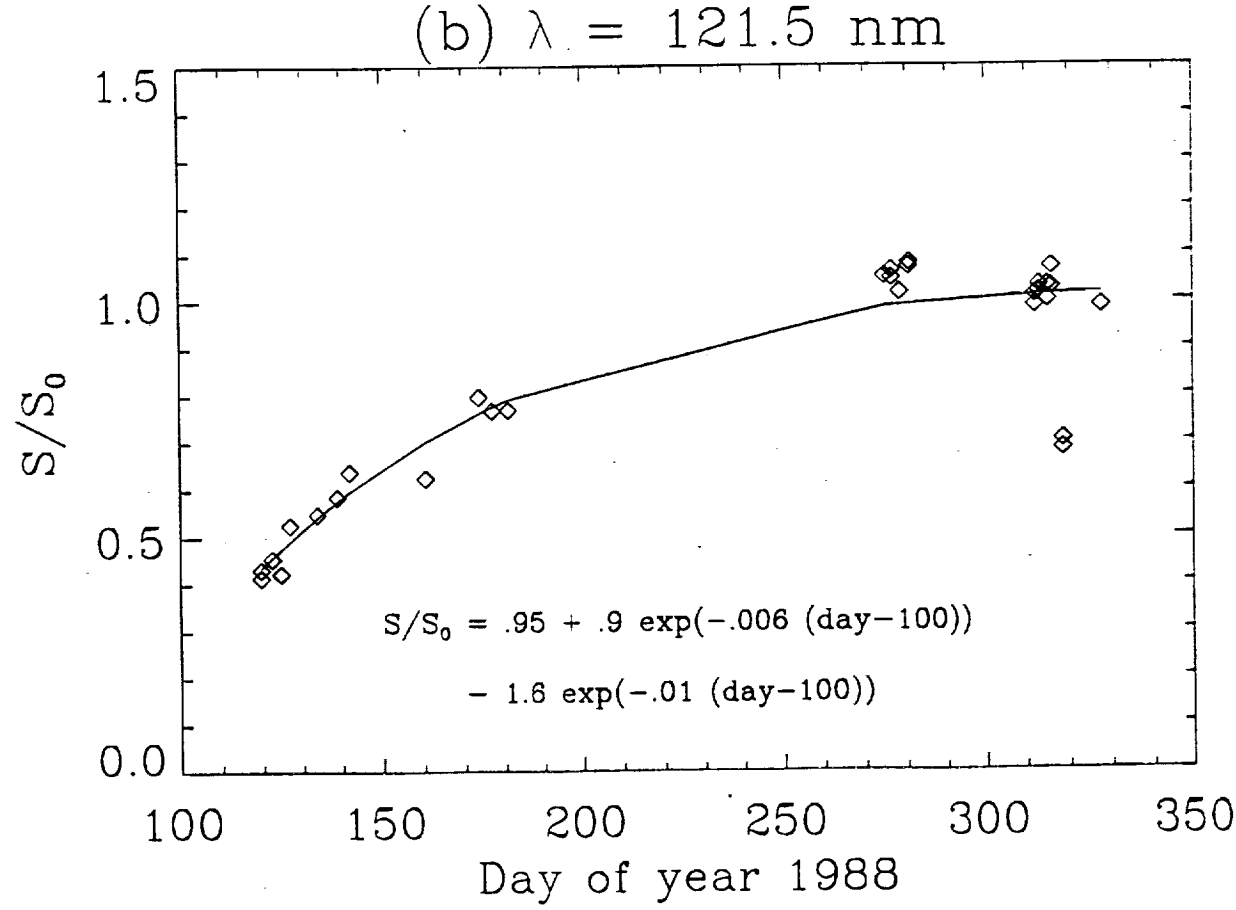
(b) λ = 121.5 nm
1.5
1.0
0.5
0.0
S/S0
S/S0 = .95 + .9 exp(−.006 (day−100))
− 1.6 exp(−.01 (day−100))
100
150
200
250
300
350
Day of year 1988

Fig 5

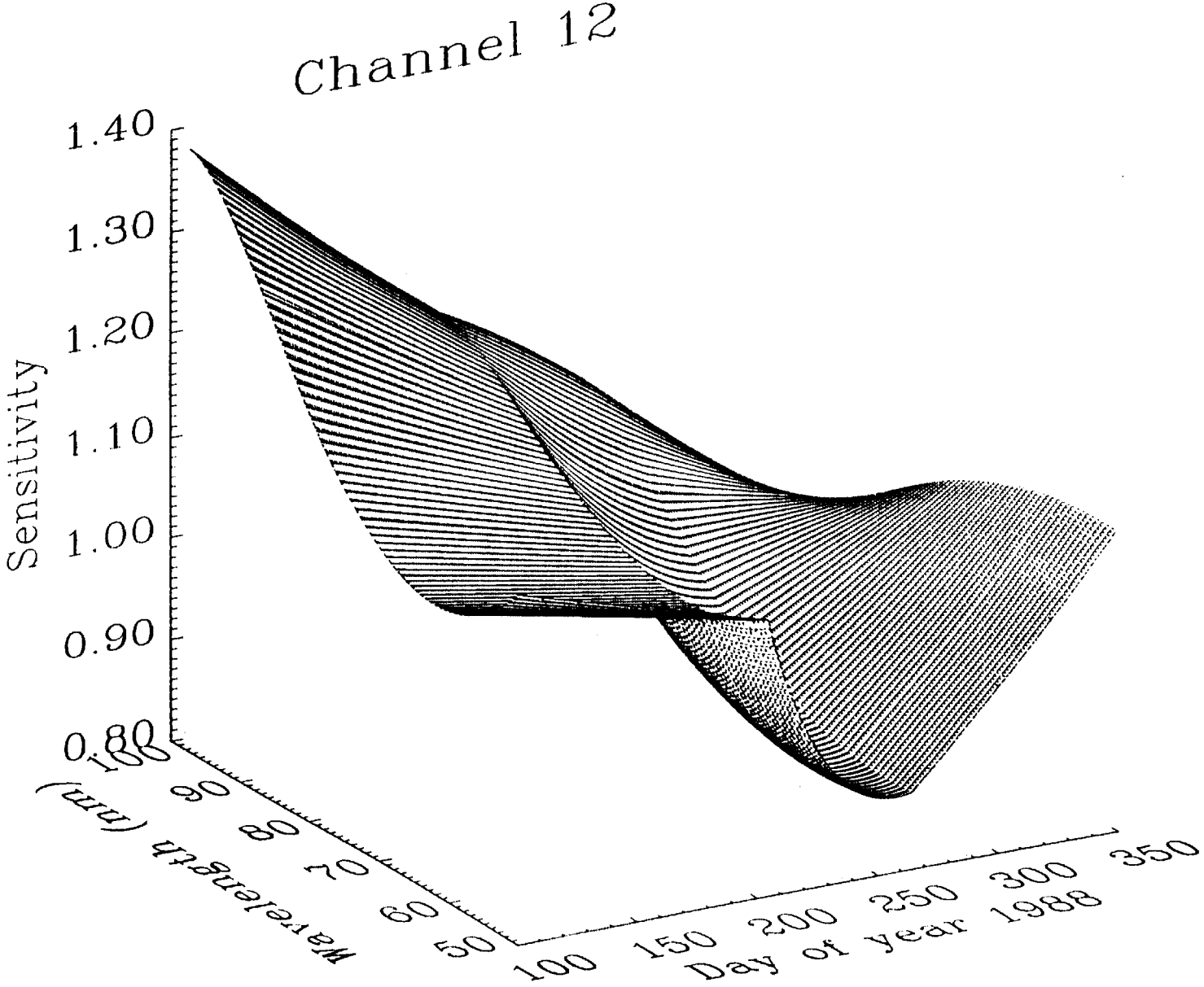
Channel 12
Sensitivity
1.40
1.30
1.20
1.10
1.00
0.90
0.80
Wavelength (nm)
100
90
80
70
60
50
100
150
200
250
300
350
Day of year 1988

Fig 6a

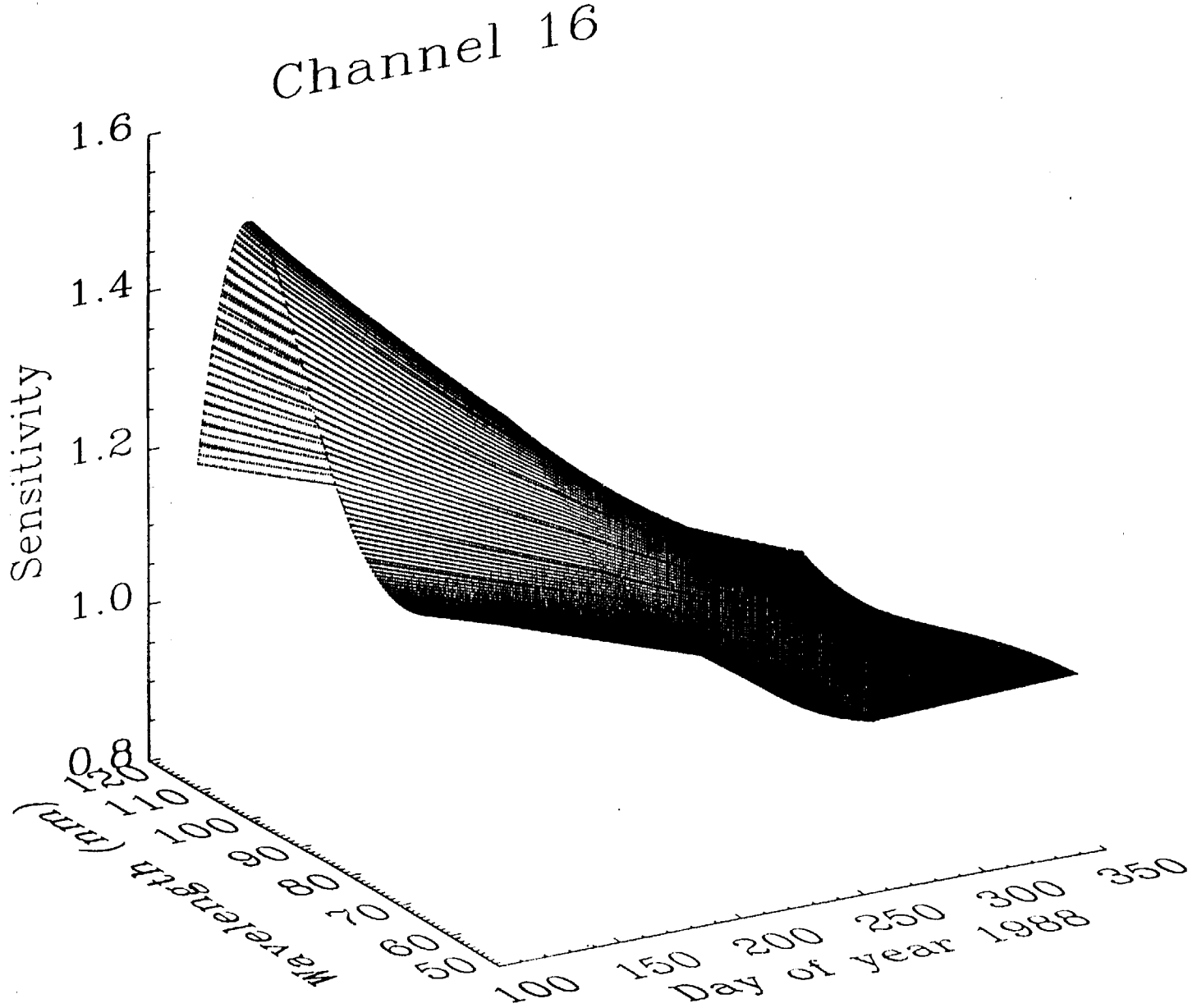
Channel 16
Sensitivity
1.6
1.4
1.2
1.0
0.8
Wavelength (nm)
120
110
100
90
80
70
60
50
100
150
200
250
300
350
Day of year 1988

Fig 6b

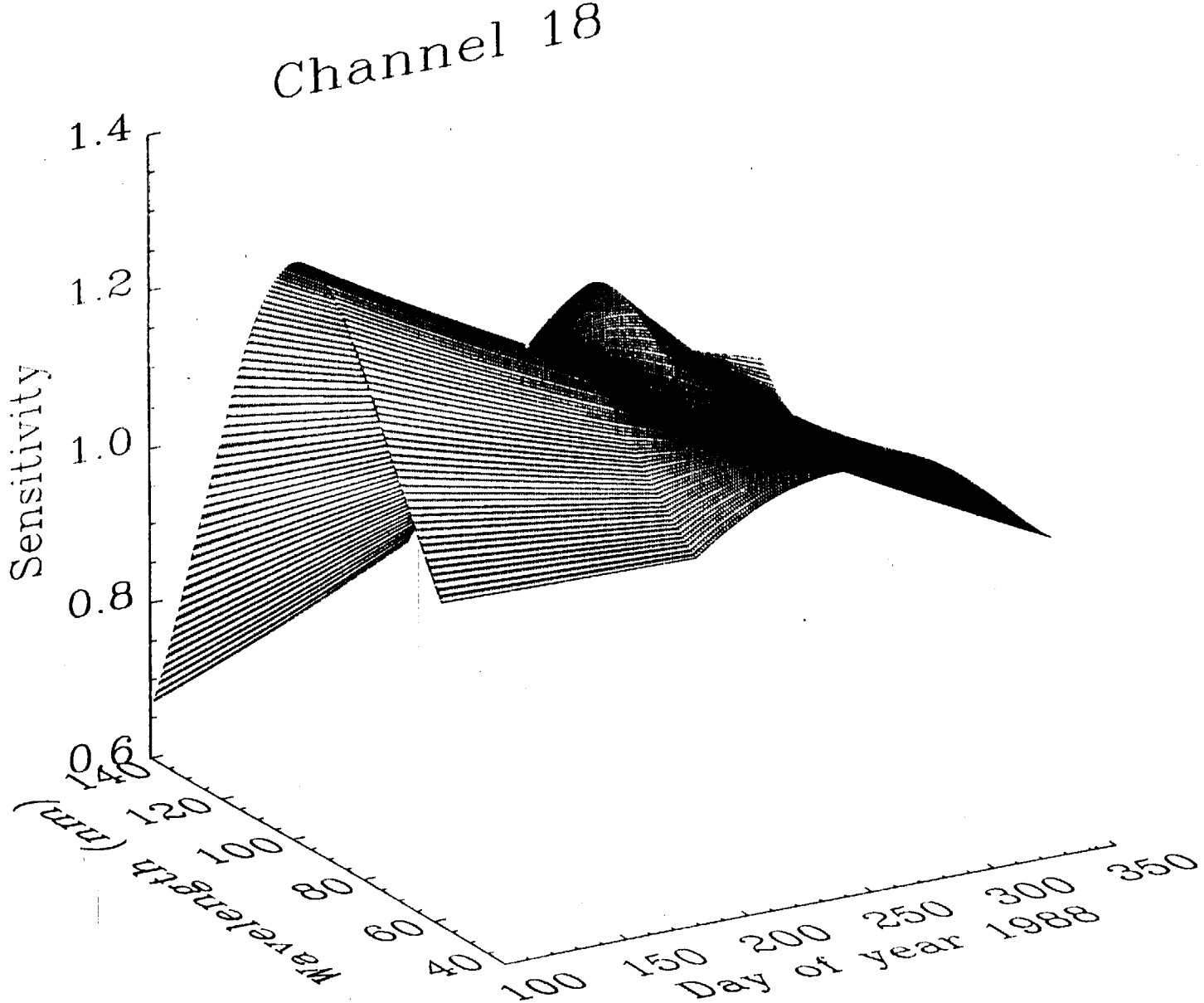
Channel 18
Sensitivity
1.4
1.2
1.0
0.8
0.6
140
120
100
80
60
40
Wavelength (nm)
100
150
200
250
300
350
Day of year 1988

Fig 6c

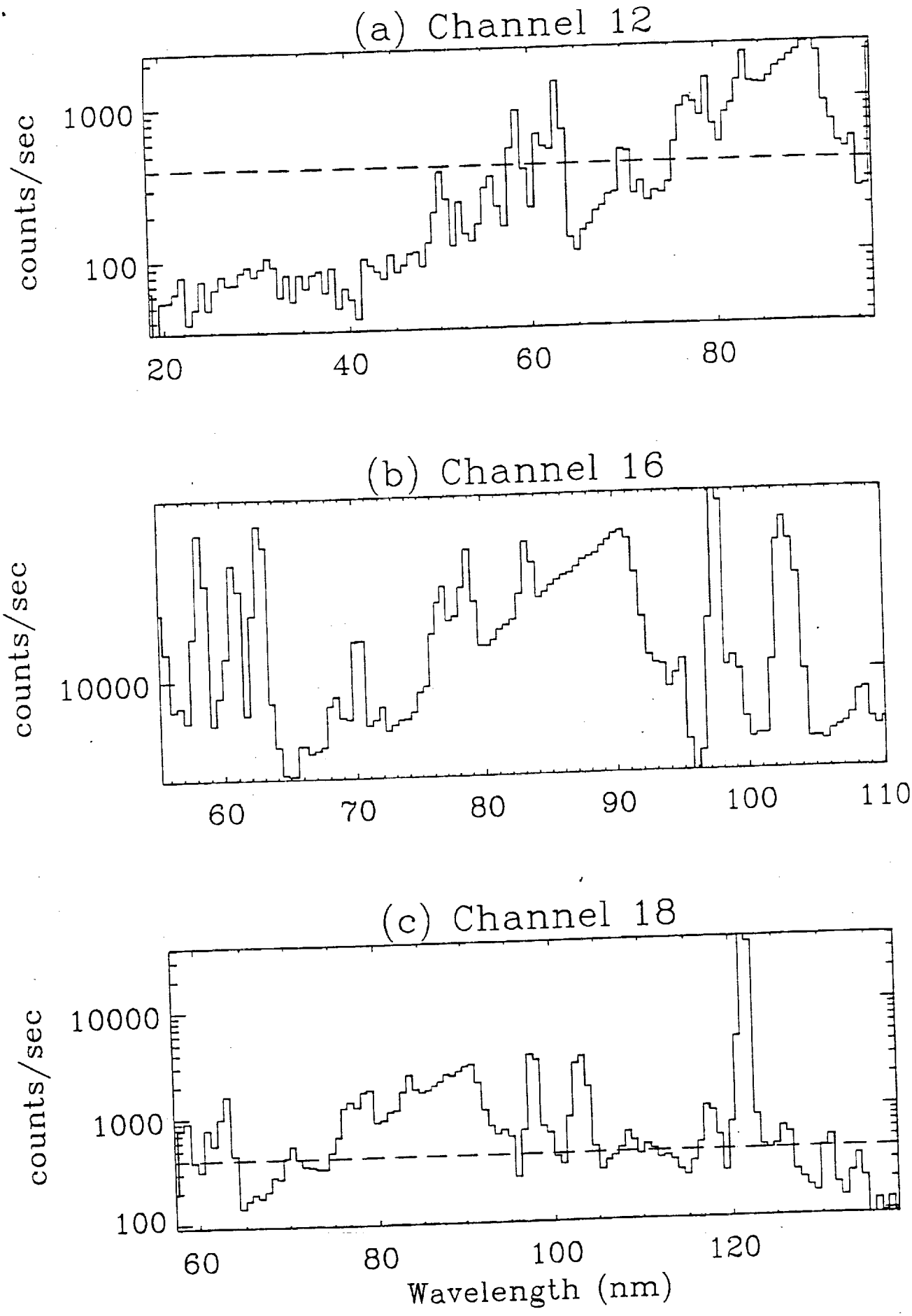
(a) Channel 12
counts/sec
1000
100
20
40
60
80
(b) Channel 16
counts/sec
10000
60
70
80
90
100
110
(c) Channel 18
counts/sec
10000
1000
100
60
80
100
120
Wavelength (nm)

Fig 7

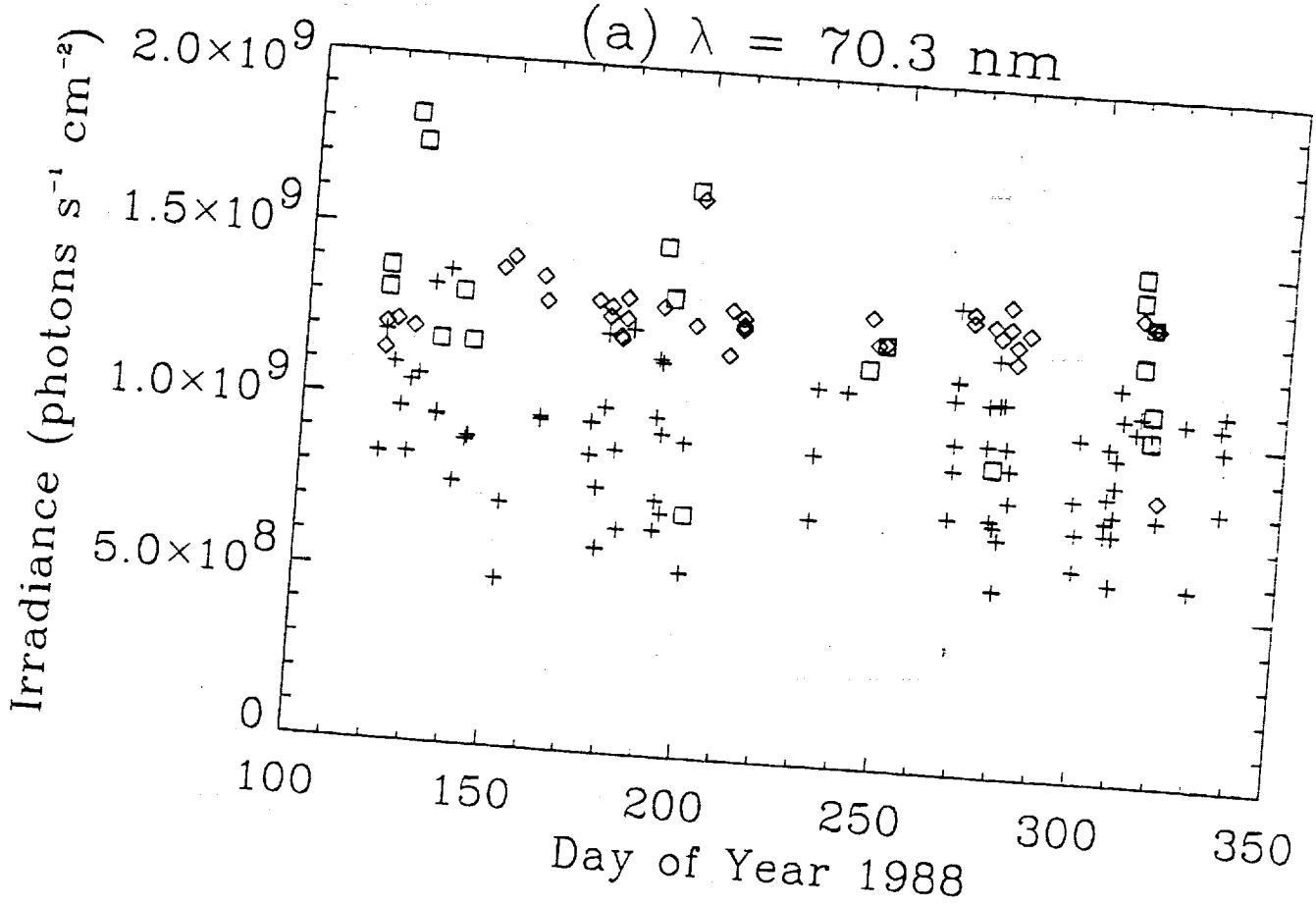
(a) λ = 70.3 nm
Irradiance (photons s⁻¹ cm⁻²)
2.0×10⁹
1.5×10⁹
1.0×10⁹
5.0×10⁸
0
100
150
200
250
300
350
Day of Year 1988

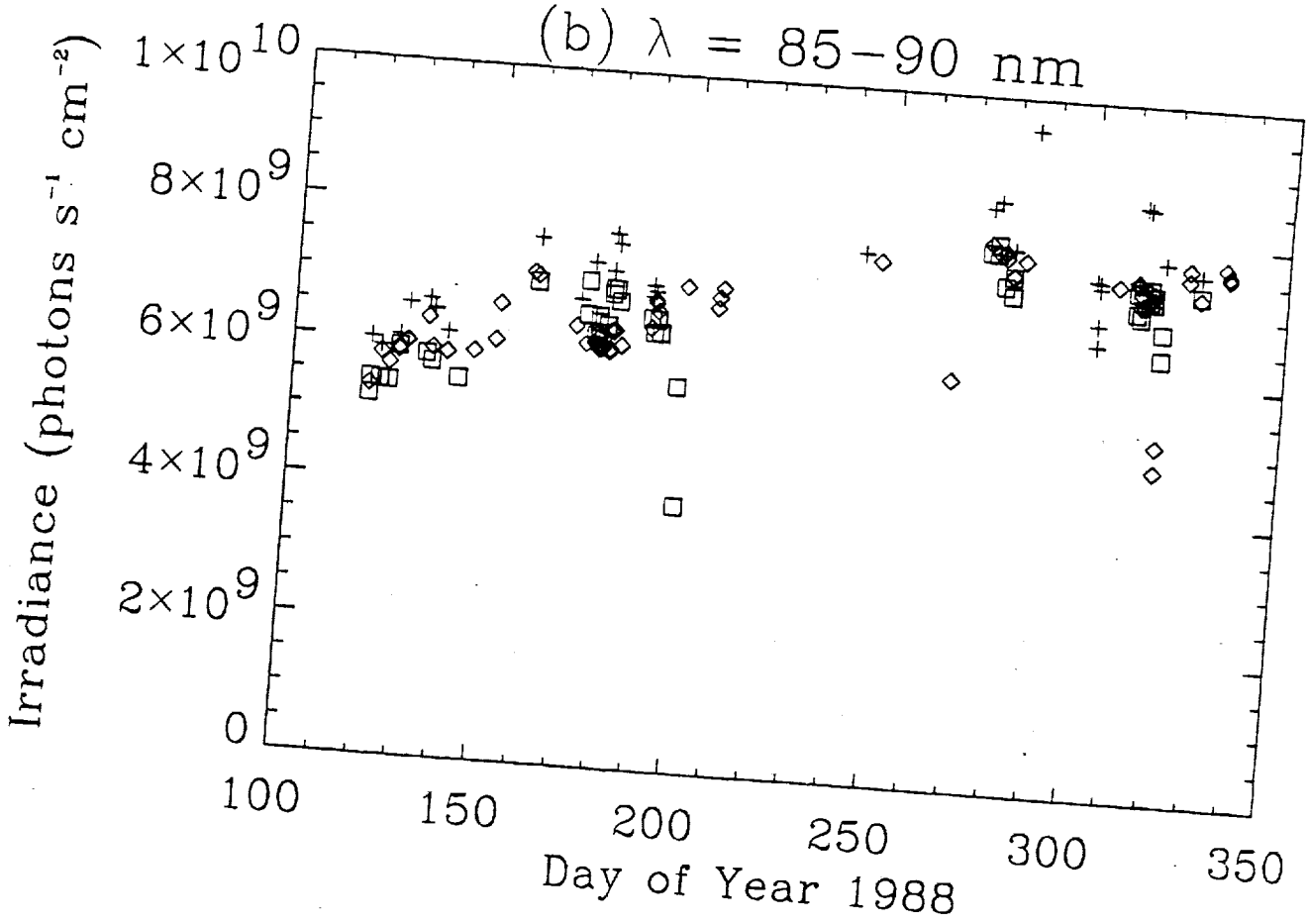
(b) λ = 85–90 nm
Irradiance (photons s⁻¹ cm⁻²)
1×10¹⁰
8×10⁹
6×10⁹
4×10⁹
2×10⁹
0
100
150
200
250
300
350
Day of Year 1988

Fig 8

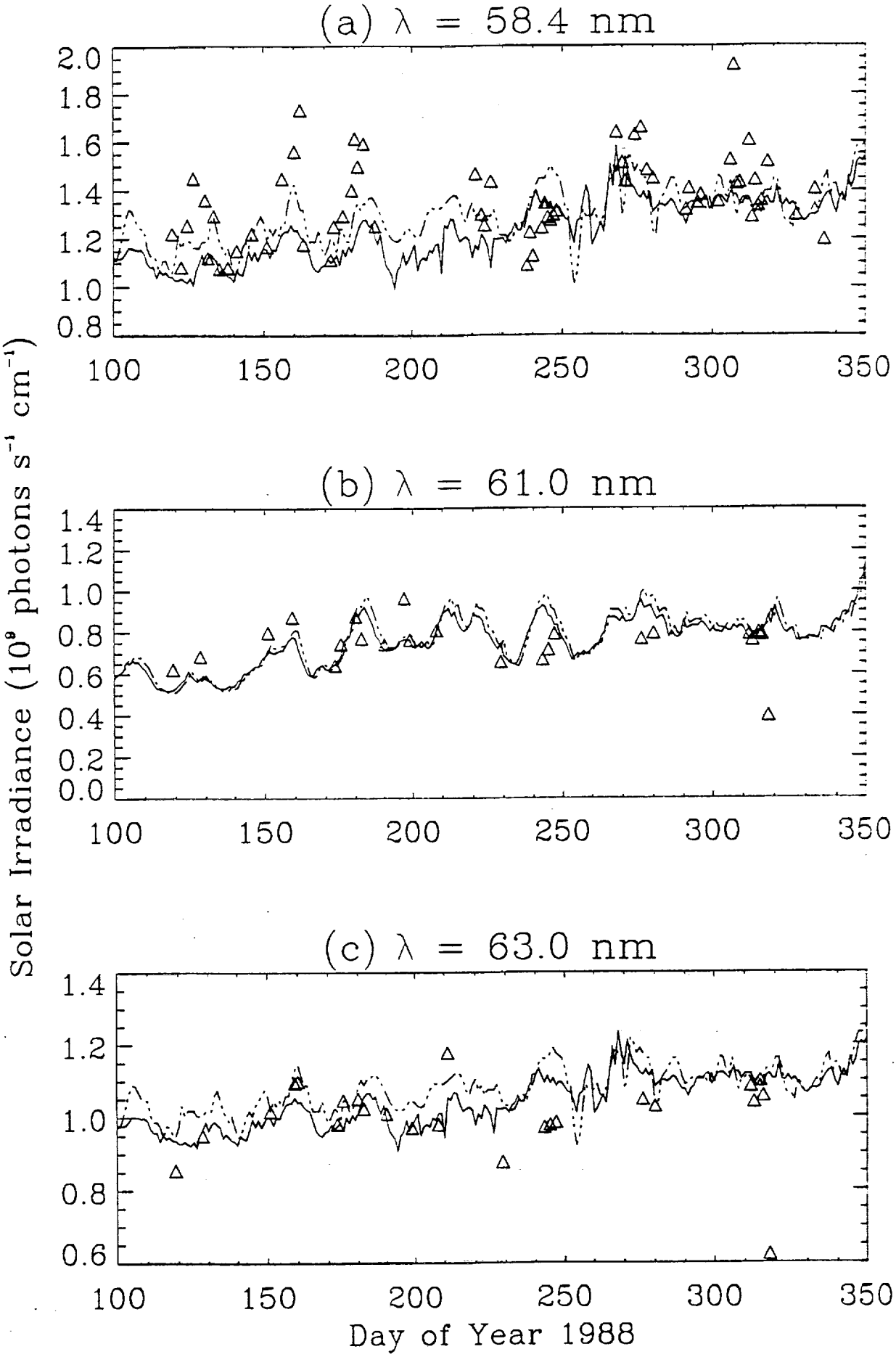
(a) λ = 58.4 nm
(b) λ = 61.0 nm
(c) λ = 63.0 nm
Solar Irradiance (10^9 photons s^{-1} cm^{-1})
Day of Year 1988
2.0
1.8
1.6
1.4
1.2
1.0
0.8
0.6
0.4
0.2
0.0
100
150
200
250
300
350

Fig 9

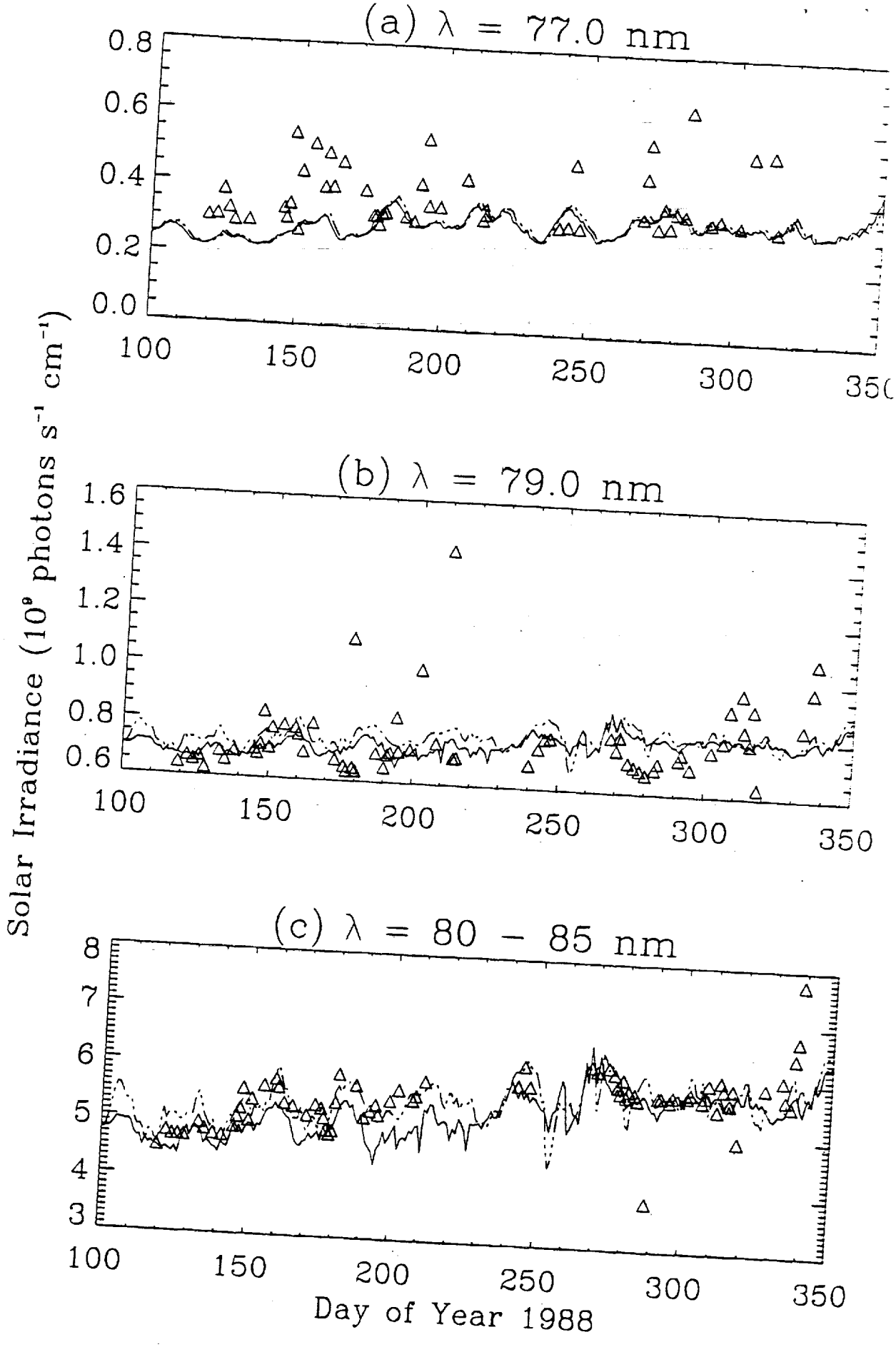
(a) λ = 77.0 nm
0.8
0.6
0.4
0.2
0.0
100
150
200
250
300
(b) λ = 79.0 nm
1.6
1.4
1.2
1.0
0.8
0.6
100
150
200
250
300
350
(c) λ = 80 – 85 nm
8
7
6
5
4
3
100
150
200
250
300
350
Day of Year 1988
Solar Irradiance (10⁹ photons s⁻¹ cm⁻¹)

Fig 10

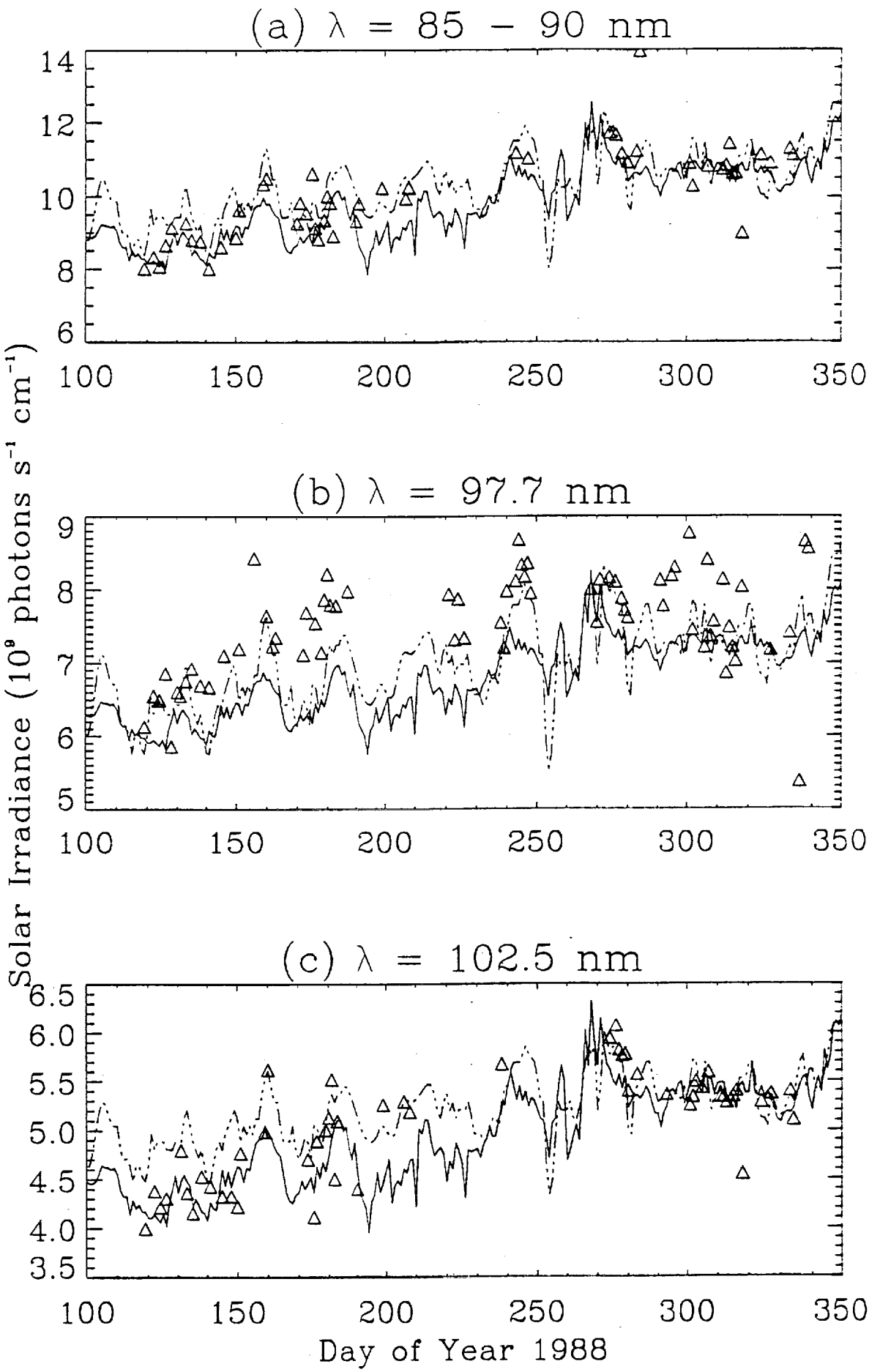
(a) λ = 85 – 90 nm
(b) λ = 97.7 nm
(c) λ = 102.5 nm
Solar Irradiance (10^9 photons s^{-1} cm^{-1})
Day of Year 1988
14
12
10
8
6
9
7
5
6.5
6.0
5.5
5.0
4.5
4.0
3.5
100
150
200
250
300
350

Fig 11